國立交通大學

電信工程學系

碩士論文

雙頻帶毫米波晶片單極天線，新型前端輻射天線及高前後輻射比之準八木天線之設計

Design of the Dual-Band Millimeter-Wave On-Chip Monopole Antenna, a Novel Structure for the End-Fire Pattern Antenna and High Front-to-Back Ratio Quasi-Yagi Antenna

研究生：黃玠瑆

指導教授：周復芳　博士

中華民國九十八年六月

雙頻帶毫米波晶片單極天線，新型前端輻射天線及高前後輻射比之準八木天線之設計

Design of the Dual-Band Millimeter-Wave On-Chip Monopole Antenna, a Novel Structure for the End-Fire Pattern Antenna and High Front-to-Back Ratio Quasi-Yagi Antenna

研究生：黃玠瑝　　Student：Jie-Huang Huang

指導教授：周復芳　博士　　Advisor： Dr. Christina F. Jou

國立交通大學

電信工程學系碩士班

碩士論文

A Thesis

Submitted to Department of Communication Engineering

College of Electrical and Computer Enginerring

National Chiao Tung University

In Partial Fulfillment of Requirements

For the Degree of

Master of Science

In Communication Engineering

June 2009

Hsinchu, Taiwan, Republic of China

中華民國九十八年六月

雙頻帶毫米波晶片單極天線，新型前端輻射天線及高前後輻射比之準八木天線之設計

研究生：黃玠瑄　　指導教授：周復芳　博士

國立交通大學電信工程學系碩士班

中文摘要

本篇論文提出三種類型天線之設計。一是晶片天線之研究，一主題是研究能產生前端輻射場型的新型架構天線，最後一主題研究則是探討高前後輻射比準八木天線。

針對第一個主題，在此我們提出一個 24 / 60GHz 雙頻帶毫米波晶片單極天線。在天線饋入部分，我們採用共平面波導之架構。由於是雙頻帶的設計，在此有兩條主要的電流路徑產生輻射。而為了避免低頻帶的高階模頻帶的出現，我們加入兩條旁支帶線去耦合該頻帶。同時也使得高頻帶的效能變好。

第二個主題，在此我們提出一個新型的前端輻射架構天線。利用減少接地金屬面，加入與接地金屬形成短路的微帶金屬線以及選擇合適的位置以及適當的金屬大小，讓天線主體和接地的微帶線，兩者在相連之後，我們即可達到產生前端輻射的目的。並且，該天線之前後輻射比會隨著操作頻率的上升而逐漸增高。

而探討到第三個主題，在此我們提出一個高前後輻射比準八木天線。該天線包含三部分，一是反射元件，同時也是該天線的地，二是驅動元件，三是導向元件。在此為了提高天線增益以及前後輻射比，我們一共使用了三個導向元件。另外值得一提的是，為了提升該天線的效能，在此的驅動元件，亦即偶極天線，其中兩個雙臂並不是在相對稱的位置，兩者距離該天線的地互有遠近。其中從地延

伸出來的偶極天線的單臂，其離地的距離比從訊號路徑延伸出來的偶極天線的單臂稍微遠一些。最後，我們還提出一能有效提升前後輻射比，天線增益也大為提高的改良架構

Design of the Dual-Band Millimeter-Wave On-Chip Monopole Antenna, a Novel Structure for the End-Fire Pattern Antenna and High Front-to-Back Ratio Quasi-Yagi Antenna

Student: Jie-Huang Huang Advisor: Dr. Christina F. Jou

Department of Communication Engineering

College of Electrical and Computer Engineering

National Chiao Tung University

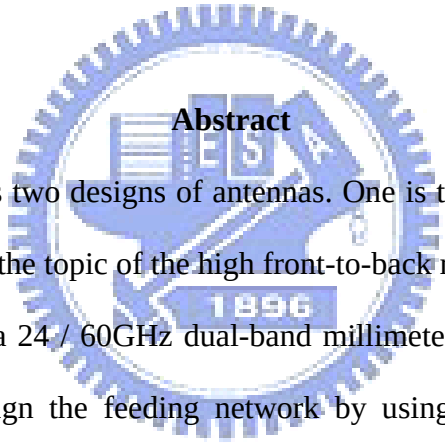

Abstract

This paper proposes two designs of antennas. One is the research of the on-chip antenna, the other one is the topic of the high front-to-back ratio quasi-Yagi antenna.

For the first topic, a 24 / 60GHz dual-band millimeter-wave on-chip antenna is presented here. We design the feeding network by using the coplanar waveguide (CPW) structure. For the dual-band design, there are two major current paths to radiate. To avoid the harmonic frequency band of the low frequency-band, we add two strips to couple the harmonic frequency of the low frequency-band. Besides, the two strips let the higher frequency-band performance better.

Then, the second topic, a novel structure for end-fire antenna, is introduced here. By the reduce the ground plane, adding short-circuited with ground stubs and choosing the appropriate position and the size of the connecting metal squares where the antenna body and the short-circuited stubs are connected, we can obtain the end-fire radiation pattern. And the front-to-back ratio of this design will increase as well as the operating frequency is increasing.

And the third topic, a high front-to-back ratio quasi-Yagi antenna is demonstrated here. The antenna consists of three parts which are the reflector, or ground of the antenna, the driver, and the directors. It has three directors of this quasi Yagi antenna to improve the antenna gain and the front-to-back ratio. Here, it is worth to be noticeable that the positions of the dipole arms are not at the symmetric location. The one extended from the ground plane is a few farther to the ground plane than the one extended from the signal path for improving the performance. At last, we will show the enhance type of the high gain and high front-to-back ratio quasi-Yagi antenna.

致　　謝

在這充滿感激的時刻當中，首要感謝的，是我的指導教授周復芳教授。在這兩年碩班研究期間，給我許多建議以及指導，讓我在研究的過程當中，順遂許多。同時，也要特別感謝指導我的學長，俊緯，在這兩年多來的時間裡，當我還在對天線這一個浩瀚無涯的學術領域感到懵懂無知的時候，不僅是在專業的學術領域之中教導我很多學業上的知識，也在求學的態度上成為我最佳的學習榜樣。感謝老師和學長這兩年來的提攜，使我得而順利在兩年內完成碩士研究。

接著要感謝 919 實驗室的各位，感謝已畢業的學長智元無論是在學業上或是生活上給予我的指導與關心。也感謝一起在實驗室裡同甘共苦的各位：蘇董，安東尼，小老鼠，跳跳虎，在職的岳昌，文斗，下一屆的學弟們以及最常和我一同苦笑的奕霖，因為有你們，在這實驗室裡總是充滿著歡笑，讓我在面對研究壓力之餘，能夠感受到我們是一起奮鬥的夥伴，也讓我更有信心去面對接下來的挑戰。感謝各位在求學路上，和我一起相互抵礪，讓我這兩年的碩班上活更加多采多姿。

此外，也要感謝國家晶片中心晶片實作組的各位主管，教導我的學長們，新進來的學弟妹們，以及陪我一起面對永遠量不完的晶片量測的同事們，在這一段時間，讓我在天線的專業領域之外，也學習到其它很多的相關知識，也讓我的生活更多添許多色彩。

另外，要感謝我的家人們，在這一段漫長的時間裡，默默地支持我完成學業。謝謝兩位妹妹，爸，媽以及奶奶的包容，讓我能無後顧之憂，專心於研究之上。

最後，還有許多曾經幫助過我的人，在這裡我要表達我對你們的謝意。在此，僅以此小小成果獻給我的家人，並與你們分享我的喜悅，謝謝！

黃玠瑾

於 風城交大

2009.06

Table of contents

Page

LIST OF TABLES

LIST OF FIGURES

Chapter 1

Introduction

1.1 Motivation

Recently, there is much interest in 60-GHz band for wireless personal area network (WPAN) application which is noticed in the short-range communications because of its attenuation characteristic of atmospheric oxygen of 10–15 dB/km in a bandwidth of about 8 GHz centered around 60 GHz [1] and [2]. Due to this reason, it is very attractive to the short-range wireless communication systems design today [3].

On the other hand, the 24GHz ISM-band is also worth to being notice because it needs not licensed. Based on the advantage, it can be a good solution for short-range wireless communication [4] and [5].

Over the past few years, a number of researchers have attempted to develop the millimeter-wave CMOS RFICs and on-chip antenna which have been studied [6]-[9]. The CMOS on-chip antennas have been presented by Chuang *ea al.* in 2007 and 2008 [1] and [2]. Hence, there has lots of research of this topic and it will be an important solution for integrated MMIC antenna.

For the second and third topics, a novel structure antenna for end-fire pattern and the high front-to-back (F/B) ratio quasi-Yagi antenna are also good researches. With the development of modern wireless communications, there are some cases such as point-to-point communication systems require unidirectional radiation patterns. It is well known from antenna theory that Yagi-Uda antenna is primarily used to achieve end-fire radiation pattern by satisfying the special conditions or antenna array system is also another solution for the same situation.

Recently, the end-fire pattern antenna [10] has become a major candidate for these

applications especially the quasi-Yagi antenna because of its several advantages [11]-[19]. With the development of modern wireless communications, the end-fire radiated antenna has become a significant research in many cases like point-to-point communication systems which requires the unidirectional radiation patterns. The reason is that the end-fire radiated antenna has several advantages such as high directivity and low-cost, moreover, we can even obtain a high F/B ratio pattern which is synonymous to high unidirectional characteristic by adjusting the configuration of the antenna. Besides, it is worth noticing that the F/B ratio is an especially significant parameter in the framework of the indoor communication applications. Because it may crave to have antennas which propagate their signal primarily towards the interior of a building not only for the security but also in order to avoid waste of energy.

1.2 Organization

This dissertation has two research topics, which is organized as follows:

In chapter 1, we will introduce this dissertation at beginning and describes the motivation of this paper.

In chapter 2, we will present the on-chip antenna structure. And before that, we will review some basic theories such as half-wave dipole, image theory, and monopole. Then we begin to develop our first topic, or dual-band millimeter-wave on-chip monopole antenna.

Next, in chapter 3, we will demonstrate a novel structure for the end-fire pattern antenna. Firstly, we will introduce some antenna type whose radiation pattern is end-fire. And then, we will show the results of this design.

Then, in chapter 4, the design of the high F/B ratio quasi-Yagi antenna has been presented. Here, we will review the theory of the Yagi-Uda antenna first. And then, we will demonstrate our study of the high F/B ratio quasi-Yagi antenna. After introduction of the high F/B ratio quasi-Yagi antenna, we will present the enhance type high F/B ratio quasi-Yagi antenna.

The last, chapter 5, we will give the summary and the conclusion of all and the future study.

Chapter 2

A 24/60GHz Dual-Band Millimeter-Wave On-Chip Monopole Antenna

In this chapter, a 24 / 60GHz dual-band millimeter-wave on-chip antenna is presented here. We design the feeding network by using the coplanar waveguide (CPW) structure. For the dual-band design, there are two major current paths to radiate. To avoid the harmonic frequency band of the low frequency-band, we add two strips to couple the harmonic frequency of the low frequency-band. Besides, the two strips let the higher frequency-band performance better. At this work, the simulator is based 3-D full-wave EM solver, Ansoft HFSS. Here, we will display the simulation result of this design.

2.1 *Basic Theory*

2.1.1 *Theory of the Coplanar Waveguide (CPW) Structure*

In recent years, the CPW structure, or the GSG for the single input or GSGSG for the differential input, is very widely used in the feed structure of the MMIC or RFIC system because of its several advantages.

A coplanar waveguide (CPW) fabricated on a dielectric substrate was first demonstrated by C. P. Wen [20] in 1969. Since that time, tremendous progress has been made in CPW based microwave integrated circuits (MICs) as well as monolithic microwave integrated circuits (MMICs) [21]-[24]. A conventional CPW on a dielectric substrate consists of a center strip conductor with semi-infinite ground planes on either side shown in Fig. 2.1.

The CPW offers several advantages over conventional microstrip line:

The first is that it simplifies fabrication, which no any metal on the back side and all the metal are on the same plane. That is to say it eliminates the need for wraparound and via holes [25] and [26].

Second, a ground plane exists between any two adjacent lines so cross talk effects between adjacent lines are very week [25] and the CPW has low dispersion and hence offers the potential to construct wide band circuits and components.

Third, the characteristic impedance is determined by the ratio of the signal path metal width *s,* or 2*a* in the figure, and the distance of the two ground plane *s*+2*w*, or 2*b* in the figure, shown in Fig. 2.2, so size reduction is possible without limit, the only penalty being higher losses [27].

And the forth, it reduces radiation loss when delivering the signal by CPW structure. So it is very appropriate to being the feed network of the antenna.

According these advantages of the CPW structure, hence we use the CPW structure to being the feed structure of the on-chip antenna in this paper.

The characteristic impedance is determined by the width of the signal line and the width of the gap on either side, which the approximate formula is shown below [26].

$$Z_0 = \frac{30\pi}{K(k)/K(k')} \cdot \frac{1}{\sqrt{\varepsilon_{re}}} \tag{2.1}$$

Where ε_{re} is the effective dielectric constant of the CPW structure. The approximate formula of the effective dielectric constant can be written that

$$\varepsilon_{re} = \frac{1+\varepsilon_r}{2}(\tanh(1.785\log(h/w)+1.75)+\frac{kw}{h}(0.04-0.7k+0.01(1-0.1\varepsilon_r)(0.25+k))) \tag{2.2}$$

Where

$$k = \frac{S}{S+2W} \tag{2.3}$$

$$k' = \sqrt{1-k^2} \tag{2.4}$$

$$\begin{cases} \frac{K(k)}{K(k')} = \frac{\pi}{\ln(2\cdot\frac{1+\sqrt{k'}}{1-\sqrt{k'}})} \quad \text{for } 0 \le k \le 1/\sqrt{2} \\ \frac{K(k)}{K(k')} = \frac{1}{\pi}\ln(2\cdot\frac{1+\sqrt{k}}{1-\sqrt{k}}) \quad \text{for } 1/\sqrt{2} \le k \le 1 \end{cases} \tag{2.5}$$

If the thick of the substrate is approximately infinite, the effective dielectric constant can be written as

$$\varepsilon_{re} = \frac{1+\varepsilon_r}{2} \tag{2.6}$$

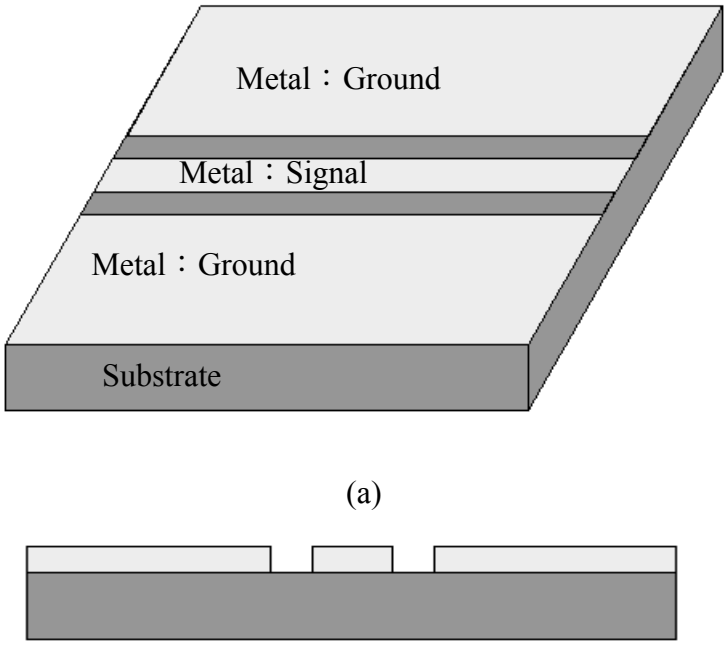

Fig. 2.1 The conventional coplanar waveguide (CPW) structure (a) 3D structure and (b) cross-section view

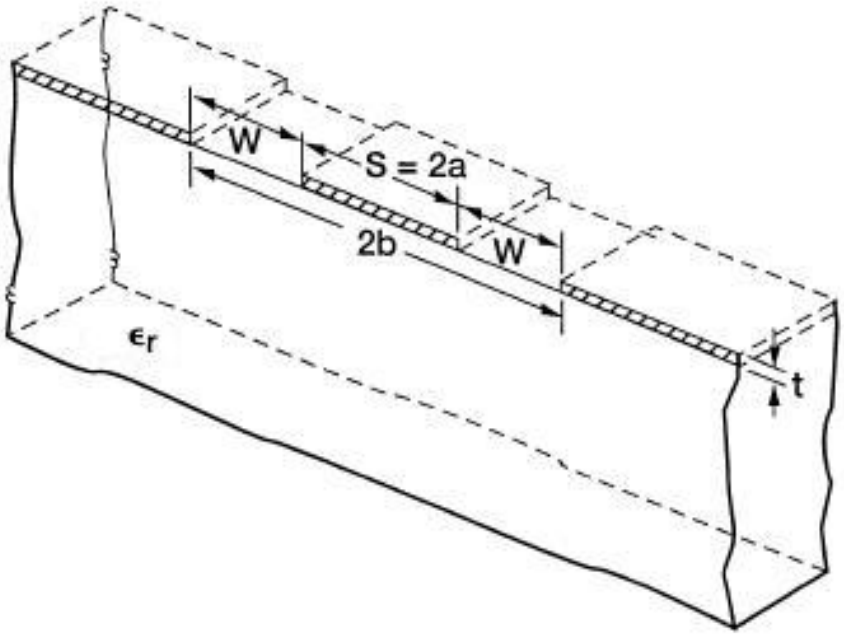

Fig. 2.2 The design parameters of the conventional CPW structure[28]

2.1.2 Theory of Half-Wave Dipole Antenna[29]-[31]

In dipole antenna, the very widely used antenna is the half-wave dipole antenna whose structure is shown in Fig. 2.3(a). It is a linear current whose amplitude varies as one-half of a sine wave with the maximum at the center of the half-wave dipole antenna and the current distribution is shown in Fig. 2.3(a). And then the radiation pattern is shown in Fig. 2.3(b). The current distribution is placed along the z-axis and for the half-sine wave current on the half-wave dipole, the current distribution can be written as

$$I(z) = I_m \sin[\beta(\frac{\lambda}{4} - |z|)], \qquad |z| \le \frac{\lambda}{4} \tag{2.7}$$

Where $\beta=2\pi/\lambda$, λ is the wavelength of the operating frequency of the antenna.

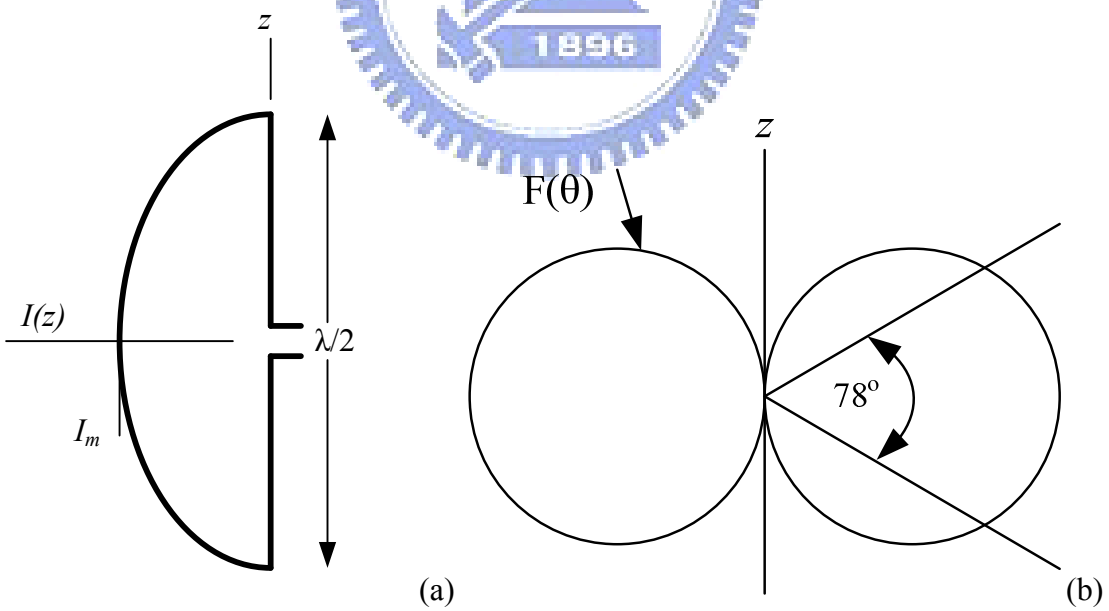

Fig. 2.3 The half-wave dipole

(a) Current distribution *I(z)* and (b) Far-field radiation pattern *F(θ)*

This current will have the maximum value I_m at the center ($z=0$) and will be zero at the ends ($z=\pm\frac{\lambda}{4}$). According to the current distribution, the far-field radiation pattern can be calculated as

$$E_\theta = j\eta \frac{I_m e^{-\beta r}}{2\pi r}\left[\frac{\cos(\frac{\pi}{2}\cos\theta)}{\sin\theta}\right] \tag{2.8}$$

$$H_\phi = j\frac{I_m e^{-\beta r}}{2\pi r}\left[\frac{\cos(\frac{\pi}{2}\cos\theta)}{\sin\theta}\right] \tag{2.9}$$

$$E_\phi = H_\theta = 0 \tag{2.10}$$

The definition of the field pattern function, *F(θ)=g(θ)f(θ)*, then the complete (normalized) far-field pattern of the half-wave dipole antenna is

$$F(\theta) = \frac{\cos[(\pi/2)\cos\theta]}{\sin\theta} \qquad \textit{half-wave dipole} \tag{2.11}$$

And then we define the antenna directivity, *D*, which defines as that:

$$D = \frac{U_{\max}}{P_{rad}/4\pi} \tag{2.12}$$

In theory, the input power can be radiated totally by antenna. In practical, the antenna has the loss, however, the radiated power will less than the input power. Because of this reason, we define the antenna radiation efficiency, η_r, and the antenna

gain, G, which are defined as

$$\eta_r = \frac{P_{rad}}{P_{in}} \tag{2.13}$$

Note that

$$0 \le \eta_r \le 1 \tag{2.14}$$

And the antenna gain is

$$G = \eta_r \times D \tag{2.15}$$

Since gain is a power ratio it can be calculated in decibels as follows

$$G_{dB} = 10 \log G \tag{2.16}$$

$$D_{dB} = 10 \log D \tag{2.17}$$

Gain relative to a half-wave dipole carries the units of dBd. And the unit dBi is often used instead of dB to emphasize that an isotropic antenna is the reference. The relation between the dBi and the dBd is:

$$dBi = dBd + 2.15 \tag{2.18}$$

According to the antenna parameters mentioned above, we can know that the radiation efficiency is the higher the better. That is to say the input power can radiate

by antenna almost and then the antenna gain will be higher.

2.1.3 Theory of the Image Theory[29]-[31]

Consider an ideal dipole near a perfect ground plane and oriented perpendicular to the ground plane shown in Fig. 2.4. The uniqueness of the solution to a differential equation (wave equation) plus its boundary conditions introduces an equivalent system that is different below the ground plane (GG'). However, it satisfies the same boundary conditions on the ground plane (GG') and has the same sources above the plane. Using this equivalent model, the solution will be different for the initial problem which below the plane. However, we can find the same solution for the problem above the ground plane and satisfies the boundary conditions. As a result, the image for this case is equidistant below the image plane and the same direction.

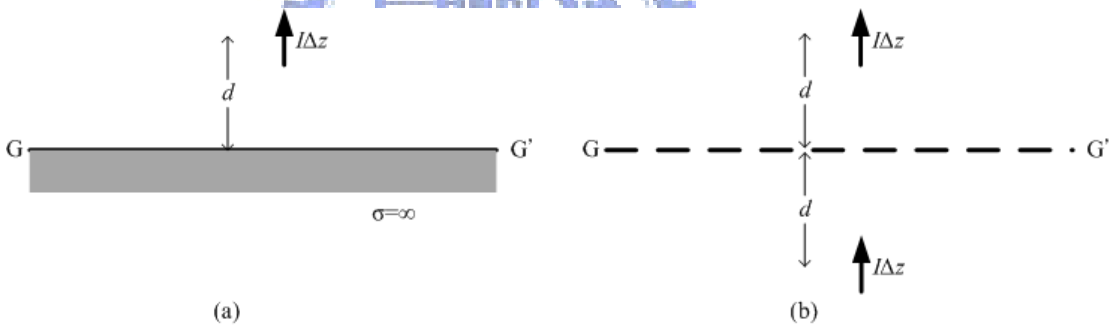

Fig. 2.4 Ideal dipole above and perpendicular to a perfectly conducting ground plane

(a) Physical model and (b) Equivalent model using image theory

An ideal dipole oriented parallel to a perfect ground plane has an image that again is equidistant below the image plane. However, the direction is oppositely as shown in Fig. 2.5.

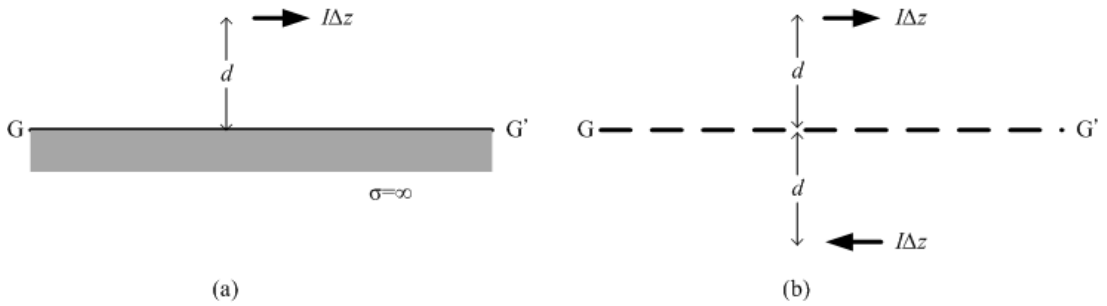

Fig. 2.5 Ideal dipole above and parallel to a perfectly ground plane

(a) Physical model and (b) Equivalent model using image theory

The image of a current element oriented in any direction with respect to a perfect ground plane can be calculated by decomposing the element into perpendicular and parallel components, shaping the images of the components, and constructing the image from these image components as shown in Fig. 2.6.

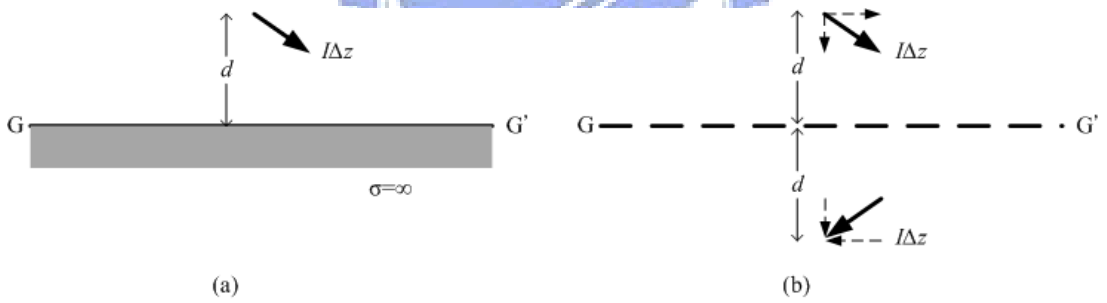

Fig. 2.6 Ideal dipole above and obliquely oriented relative to a perfectly ground plane

(a) Physical model and (b) Equivalent model using image theory

2.1.4 Theory of the Monopole[29]-[31]

A monopole is a dipole that has been divided in half at its center feed point and fed against a ground plane shown in Fig. 2.7. According to the image theory, if the current distribution over the monopole antenna is equal to the dipole then the electric

field of the monopole and the dipole will be the same. However, the image current of the monopole is generated by the ground metal. Hence, the length of the monopole is one-quarter wavelength, which is half of the dipole.

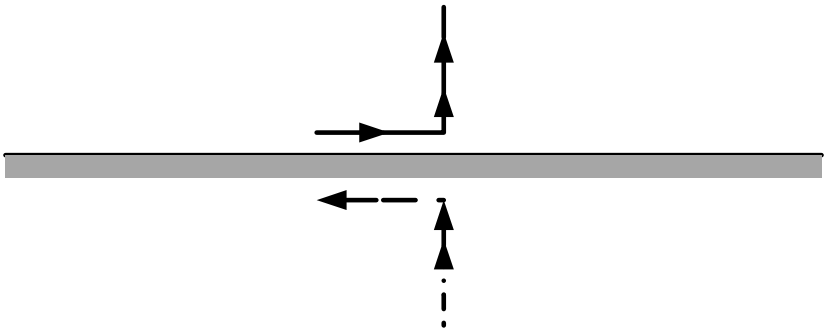

Fig. 2.7 Monopole antenna over perfect ground plane with their image (dashed)

The current and charges on a monopole are the same as on the upper half of its dipole counterpart, but the terminal voltage is only half that of the dipole. The input impedance for a monopole is half of its dipole counterpart, or

$$Z_{A,mono} = \frac{V_{A,mono}}{I_{A,mono}} = \frac{\frac{1}{2}V_{A,dipole}}{I_{A,dipole}} = \frac{1}{2}Z_{A,dipole} \tag{2.19}$$

Where $Z_{A,mono}$ is the input impedance of the monopole and $Z_{A,dipole}$ is for dipole. Therefore, the radiation resistance of the monopole can be written as:

$$R_{r,mono} = \frac{P_{mono}}{\frac{1}{2}\left|I_{A,mono}\right|^2} = \frac{\frac{1}{2}P_{dipole}}{\frac{1}{2}\left|I_{A,dipole}\right|^2} = \frac{1}{2}R_{r,dipole} \tag{2.20}$$

Where $R_{r,mono}$ is the radiation resistance of the monopole and $R_{r,dipole}$ is for dipole.

The radiation pattern of the monopole above a perfect ground plane is the same

as a dipole. However, a monopole fed against a perfect ground plane radiates one-half the total power of a similar dipole in free space. Because of the reason, it is leading to a doubling of the directivity:

$$D_{mono} = \frac{4\pi}{\Omega_{A,mono}} = \frac{4\pi}{\frac{1}{2}\Omega_{A,dipole}} = 2D_{dipole} \tag{2.21}$$

Where D_{mono} is the directivity and D_{dipole} is for dipole.

2.2 Design of the 24 / 60 GHz Dual-Band Millimeter-Wave On-Chip Monopole Antenna

The structure of the proposed dual-band millimeter-wave on-chip CMOS antenna is shown in Fig. 2.8 and the layout photo of the on-chip antenna is shown in Fig. 2.9. The used process of this on-chip antenna is TSMC 0.13 CMOS process. The CPW line structure is adopted for feeding network of this antenna [1] and [2]. The structure consists of three parts: longer path monopole antenna, shorter path monopole antenna, and two stubs at the middle.

The longer current path which is near a loop and about quarter wavelength of the lower operating frequency operates at low frequency band. On the contrary, the shorter current path which is on the right side of this antenna and approximated quarter wavelength of the higher operating frequency works at high frequency band.

Here, the wavelength is the effective wavelength of the lower or higher frequency calculated by the effective dielectric constant of the substrate [32] and [33]. Besides, it is important that the distance of the CPW gap, g = 48 μm, and the distance, d = 40 μm, between the radiator and the ground metal of the CPW structure are the key factors of the matching feeding and the return loss [34].

The two strips in the middle of the antenna structure are designed by L_s = 335 μm, W_s = 30 μm, and the gap between the two stubs, s = 20 μm. The feeding line is designed by W = 80 μm. The on-chip antenna size is about 0.76 × 1.045 mm^2.

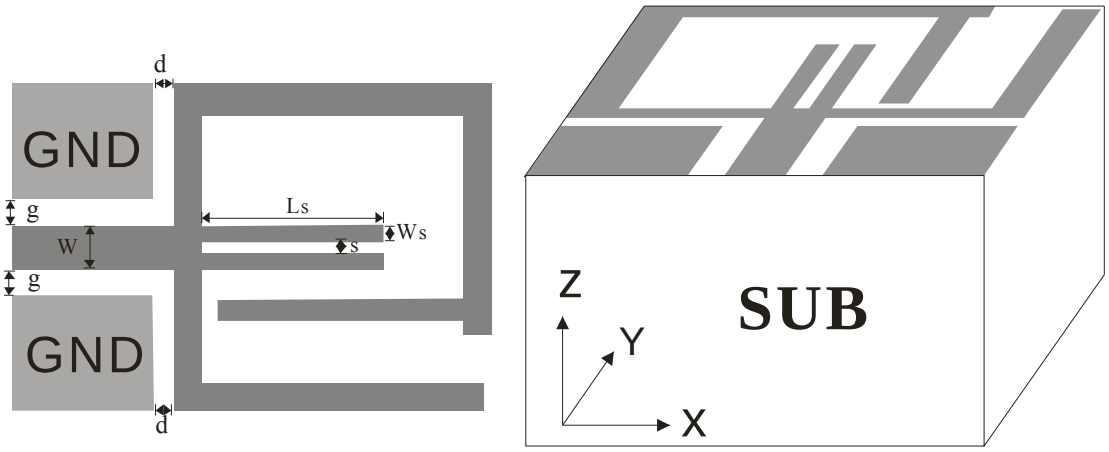

(a) (b)

Fig. 2.8 Configuration of the dual-band millimeter-wave on-chip antenna:

(a) The Geometry and (b) The 3D structure

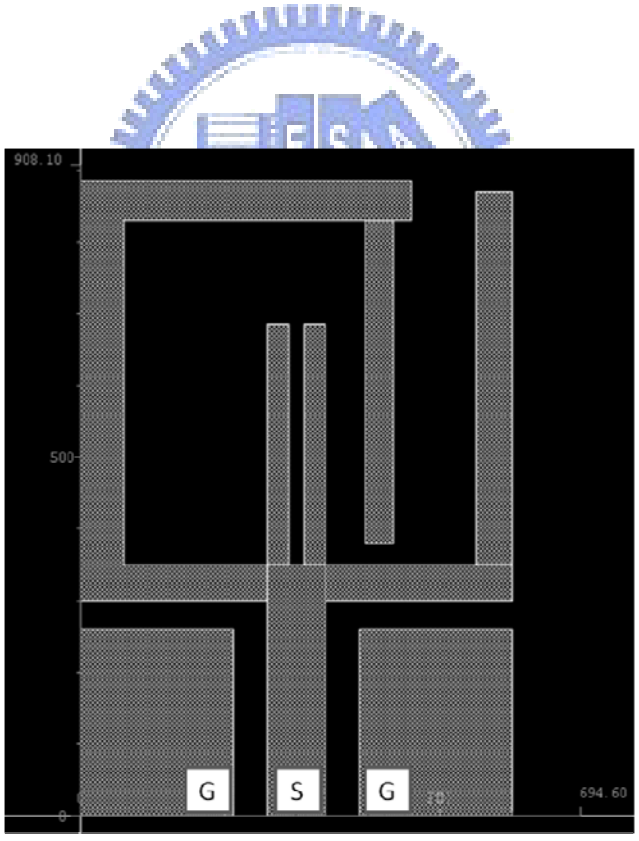

Fig. 2.9 The layout photo of the on-chip antenna

2.3 Simulation Results

The current distribution of the on-chip antenna is shown in Fig. 2.10 for operating at 24GHz and 60GHz respectively. When operating at lower band (24GHz), the main current distributes over the longer path of the on-chip antenna shown in Fig. 2.10(a). And for higher band (60GHz), the main current distributes over the shorter path of the on-chip antenna shown in Fig. 2.10(b)

Fig. 2.11 shows the simulated input return loss of the antenna. At 24GHz band, the minimum of input return loss is about 15dB and the bandwidth is about 180MHz. For the higher operating frequency band, 60GHz, the minimum of input return loss is about 38dB and the bandwidth is also about 700MHz.

For the radiation pattern at the lower operating frequency band shown in Fig. 2.12, the XY-plane approximates an omni-directional pattern and the gain is about -9dB. At this band, we can expect the pattern result by the current distribution that this antenna acts as a CPW monopole antenna. That is to say, the pattern of this antenna seems like the monopole antenna.

For higher operating frequency band, the radiation pattern shown in Fig. 2.13 has higher directivity so that the gain is about 1dB. We can see in Fig. 2.10(b) that there have two major current paths. So the pattern of this band has higher directivity. The simulated result summary is shown in Table 2.1

Table 2.1 simulated result summary

Simulated results	24 GHz band	60 GHz band
Bandwidth	180 MHz ; 0.75%	700 MHz; 1.67%
Max. gain in XY-plane	-9 dB	1 dB
Chip size	0.76 × 1.045 mm^2	

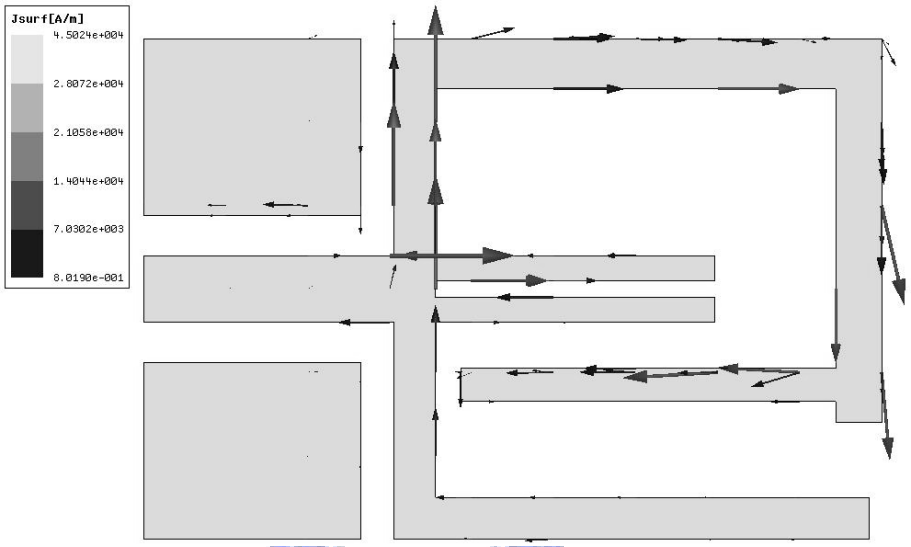

(a)

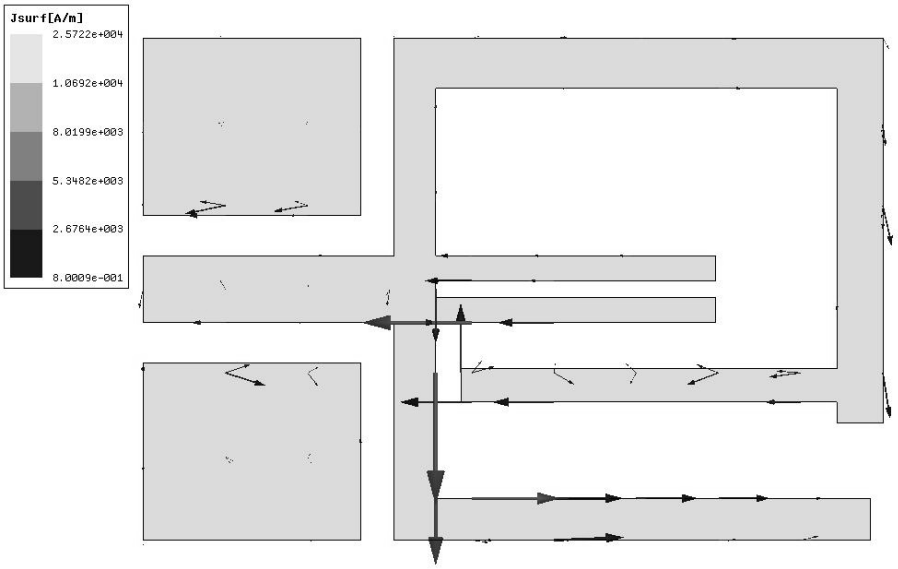

(b)

Fig. 2.10 The current distribution: (a) at 24 GHz and (b) at 60 GHz

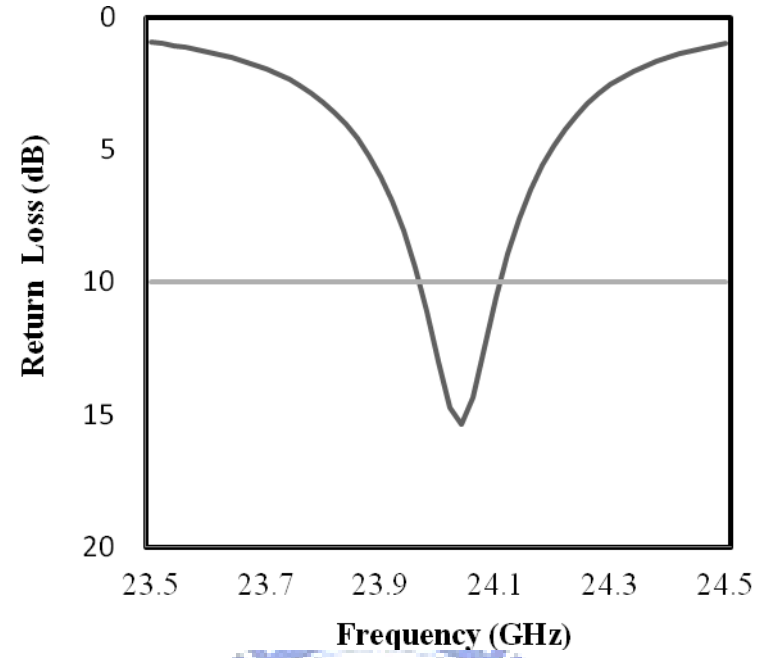

(a)

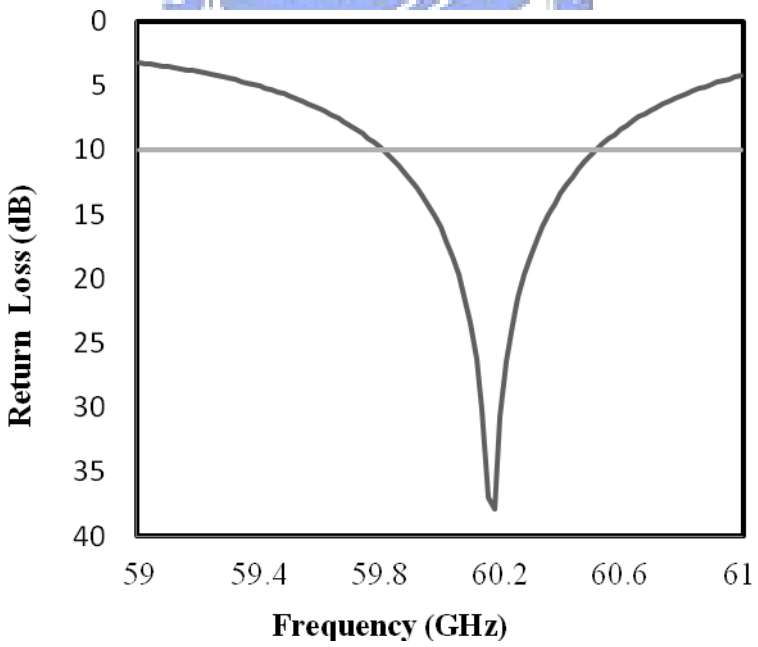

(b)

Fig. 2.11 The input return loss

(a) near the 24 GHz band and (b) near the 60 GHz band

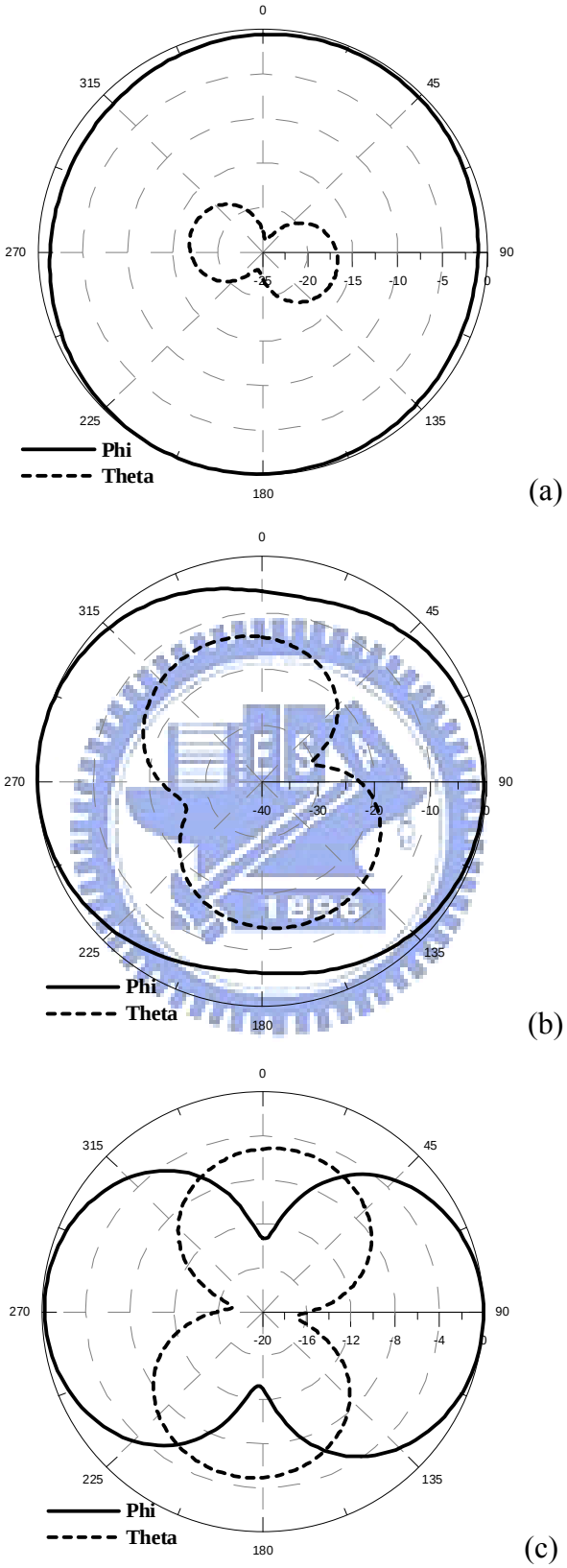

Fig. 2.12 The radiation pattern at 24 GHz

(a) The XY-plane, (b) The XZ-plane and (c) The YZ-plane

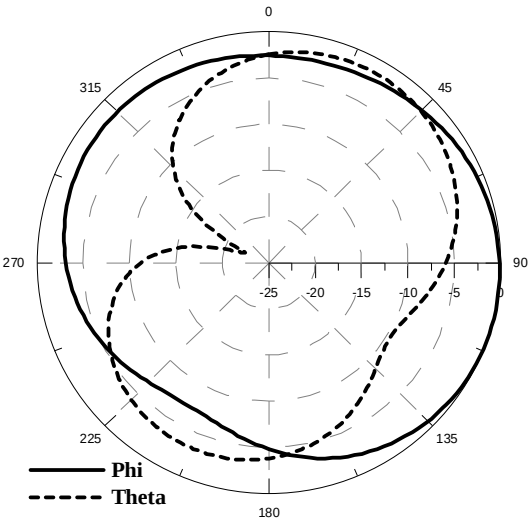

(a)

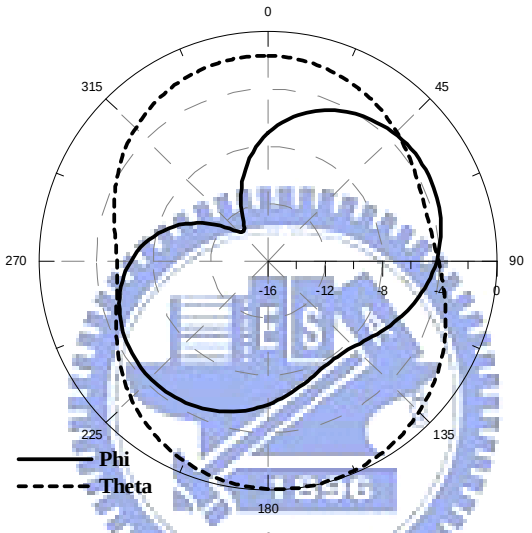

(b)

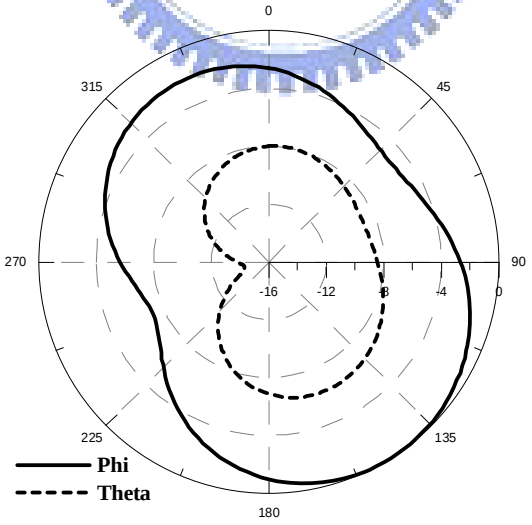

(c)

Fig. 2.13 The radiation pattern at 60 GHz

(a) The XY-plane, (b) The XZ-plane and (c) The YZ-plane

2.4 Conclusion

A 24 / 60 GHz dual-band millimeter-wave CPW-fed on-chip antenna is presented not only for a 24 GHz ISM-band application but also for 60 GHz WPAN CMOS on-chip antenna application. This on-chip CMOS antenna is fabricated with a 0.13-μm standard CMOS process. The whole on-chip antenna size is about 0.76 × 1.045 mm^2. The bandwidth of the lower band is about 0.75% and about 1.67% for higher band. The radiation pattern of the lower band approximates an omni-directional at the XY-plane and the gain is about -9 dB. For the higher band, the radiation pattern has higher directivity so the maximum gain is about 1 dB.

Chapter 3

A Novel Structure for the End-Fire Pattern Antenna

In recent years, there several antenna configurations which can provide the end-fire pattern have been proposed such as Yagi-Uda antenna [11]-[19], traveling-wave long wire antenna [35]-[36] and antenna array systems [37]-[38]. However, traditional end-fire radiated antenna is middle gain antenna and is not suitable for a radar system. In addition, most traditional end-fire antenna arrays are along z or x axes direction, which will has excellent directivity but the cross aperture figure will be limited in some special application. Therefore, it is very necessary to develop a new structure which is located along the end-fire direction, or y-axis.

In this chapter, we demonstrated a new configuration of the end-fire radiated antenna based on the leaky-wave antenna structure which has the frequency scanning characteristics that will radiate to near end-fire direction at high frequencies [39]-[42]. The proposed structure is composed of the conventional open end leaky-wave antenna with reducing ground plane and the adding short-circuited stubs and the connecting metal squares. According to the measured results, the impedance bandwidth is about 2.1GHz from 3GHz to 5.1GHz of 10-dB. The antenna peak gain we obtained is about 5.4dBi in the end-fire direction. Furthermore, the F/B ratio of this design is better than 30dB and the measurement results show that the F/B ratio is increased while the operating frequency is increased.

3.1 Some end-fire antenna structures

There are some type antennas which can obtain the end-fire radiation pattern such as Yagi-Uda antenna shown in Fig. 3.1[43], traveling-wave long wire antenna

shown in Fig. 3.2[44] and the antenna array systems shown in Fig. 3.3[45]. All of these antennas, the main operating mode is based on the array theory. Like the antenna array, the Yagi-Uda antenna structure is similar to the array but it only excides one element. For the traveling-wave long wire antenna, the current distribution of the antenna is also like the array systems.

According to the mention above, we know that the main design idea is the antenna array theory if we want design end-fire pattern antenna. In the array theory, there are many factors will affect the radiation pattern, like the distance between the each element or the excided power of each element. That is to say, we can change these factors to design the end-fire antenna.

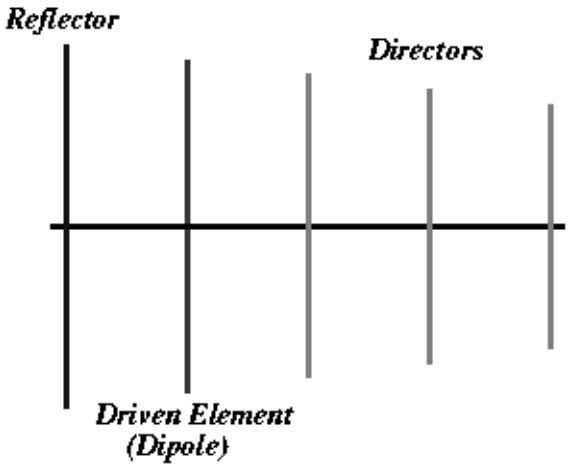

Fig. 3.1 Yagi-Uda antenna[43]

Fig. 3.2 Traveling-wave long wire antenna[44]

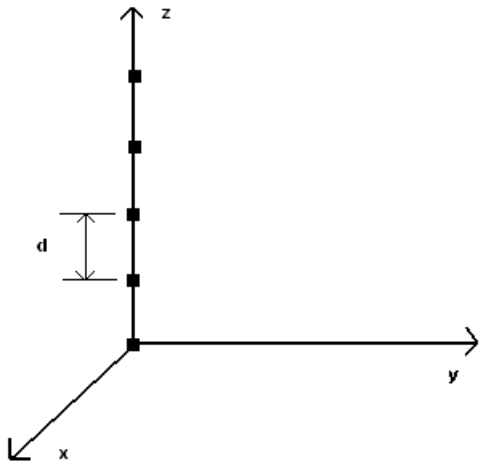

Fig. 3.3 Antenna array system[45]

3.2 The Antenna Design

Figure 3.4 shows the structure of the proposed antenna which has three parts: a) conventional open end leaky-wave antenna structure with reducing ground plane, b) adding the stubs which are connected to the ground plane and c) adding the connecting metal squares which connect the antenna body and the short-circuited stubs. These configurations are fabricated on the substrate, or FR-4, with a dielectric constant of ε_r = 4.4 and a thickness of h = 1.6mm. This research adopts an asymmetrical feed line to excite the proposed antenna which is similar to leaky-wave antenna. Detailed dimensions are listed in Table 3.1. Figure 3.4(a) shows the structure of the convention open end leaky-wave antenna of which the length L is 50mm, the width W is 15mm and the ground plane on the back side of the substrate is 45mm × 10mm.

In Fig. 3.4(b), it shows the design which we add the short-circuited stubs in order to improve the antenna gain and the impedance bandwidth. The stubs can be divided into three parts. The first stub connects to the ground plane and the distance, g_1, between this stub and the feed line is 3mm. The second stub is a vertical one which is connecting to the first stub and with the gap, g_2 = 1mm, between this stub and the antenna body. The third stub is parallel to the bottom side of the antenna body with the gap g_3 = 0.5mm and it connects to the second one. Since these stubs are short-circuited by the first stub and the gap distance between the antenna body and the third stub is very slight, it will cause that most of the current will distribute on the edges of the gap. For all the stubs, the width W_s of them are equal to 1mm and the length L_{s1} of the first stub is 14mm, the second one, or L_{s2}, is 11.5mm and the third one, or L_{s3}, is 52mm.

Figure 3.4(c) shows the configuration in which we add the connecting metal squares that connect the antenna body and the short-circuited stubs. The size of all of

the connecting metal squares is 0.5mm × 0.5mm. Here, the position and the size of the metal squares which are connecting the antenna body and the short-circuited stubs act extremely critical roles of this design. They not only match the impedance bandwidth but also affect the antenna gain and F/B ratio since the connecting metal squares will cause that the main current will be directed to the connecting metal squares between the short-circuited stubs and antenna body. That is to say, comparing configuration (b) and configuration (c), the current distribution changes from that most of the current flows on the edges of the gap to that most of current distributes at the connecting metal squares points.

Table 3.1 Dimension of the proposed antenna structure

L	50 mm	L_{s1}	14 mm	g_2	1 mm
W	15 mm	L_{s2}	11.5 mm	g_3	0.5 mm
W_g	10 mm	L_{s3}	52 mm	L_1	8 mm
W_s	1 mm	g_1	3 mm		

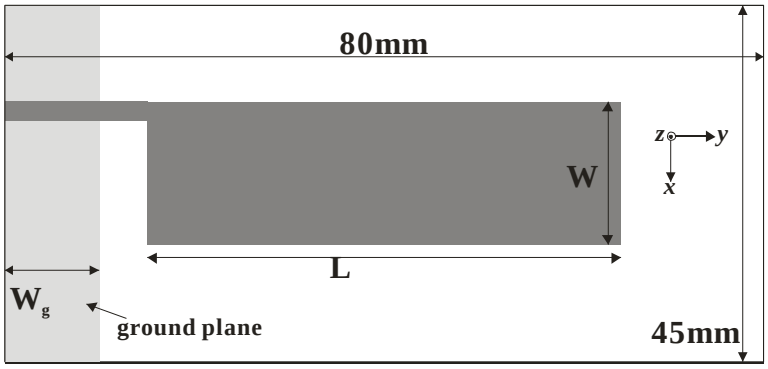

(a)

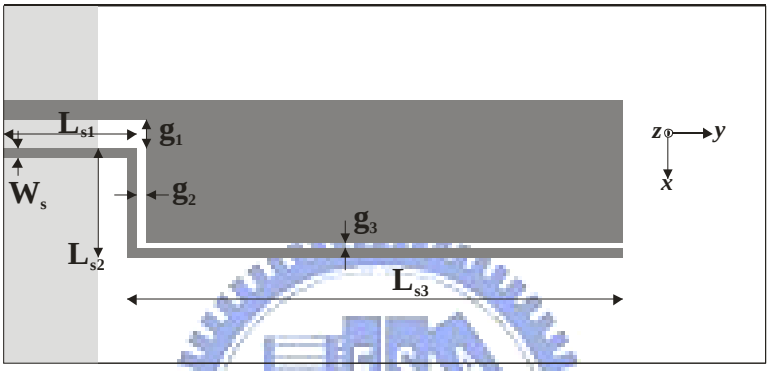

(b)

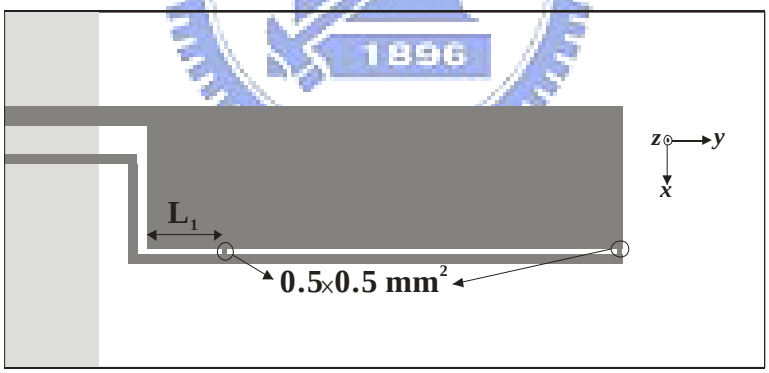

(c)

Fig. 3.4. Configuration of the proposed antenna,

(a) conventional open end leaky-wave antenna with reducing ground plane.

(b) Adding the stubs which are connected to the ground plane.

(c) Adding the connecting metal squares which connect the antenna body and the short-circuited stubs

3.3 Simulation and Measurement Results

In our study, for the original configuration which is similar to the conventional open end leaky wave antenna but the ground plane is reduced as shown in Fig. 3.4(a), we can see the current distribution in Fig. 3.5(a) which demonstrates that most of the current distributes at the bottom side of the antenna body and the current flows along the *y*-axis. Meanwhile, the length of antenna body is about a wavelength for the operating frequencies so the wave will travel on antenna body but there still has slight current which distributes on the center of the antenna body. Based on the current distribution mentioned above, the radiation pattern of this configuration will be near to the end-fire pattern in *yz*-plane, however, the F/B ratio is extremely disappointing and the antenna gain is dissatisfied because of low gain in its operating frequencies. In order to improve the antenna gain and F/B ratio, we first proposed the solution which is adding short-circuited stubs to couple the current and the fields to achieve our purpose shown in Fig. 3.4(b). However, in spite of the improvement of gain and F/B ratio, the operating band is not greatly perfect. To ameliorate the impedance bandwidth, we add two metal squares to connect the short-circuited stubs and antenna body for improving the bandwidth displayed in Fig. 3.4(c). Consequently, the impedance bandwidth has been promoted and the antenna gain and F/B ratio has also been enhanced. The detail description for these configurations will be in following subsections.

3.3.1 Adding short-circuited stubs

Figure 3.5(b) demonstrates the current distribution of the adding short-circuited stubs configuration which we can know that the current will distribute on the two sides of the gap between antenna body and stubs below the antenna mostly. As a result of the strong coupling effect, the magnitude of the current of this configuration is greatly stronger comparing to the first configuration. Because most of the current is

concentrated on two sides of the gap, the antenna gain and F/B ratio are attained improvement effectively, see Fig. 3.6(b). Here, the distance of the gap is the major relevant factor which affects the current distribution and therefore we choose the gap as 0.5mm by optimized. However, the impedance bandwidth of this configuration is dissatisfied because the return loss has inversed peak where the return loss is worse than 10-dB. For this structure, the maximum antenna gain is only 3.4 dBi and the maximum F/B ratio is just 12 dB, see Fig. 3.6(b). Owing to the imperfect performance, we present an improvement solution which is adding the metal squares connecting the antenna body and the short-circuited stubs at the particular positions.

3.3.2 Adding connecting metal squares

To improve the impedance bandwidth, we add the small size metal squares connecting the antenna body and the short-circuited stubs. For this configuration, the size and the position of the connecting metal squares will affect not only the impedance bandwidth but also antenna gain and F/B ratio. Figure 3.5(c) shows the current distribution of this structure and we can see that the main current will flow near the connecting metal squares which produce the end-fire pattern and improve the F/B ratio, see Fig. 3.6(c) and 3.6(d). The discrepancies between the simulation and the measurement results may occur because of the SMA connector and the copper metal which is connecting the stubs and the ground plane on the backside of the substrate. Since the grounded of the short-circuited stub is imperfect and the solder of SMA connector will cause the mismatch for the signal. In this configuration the maximum antenna gain is about 5.4dBi and the maximum F/B ratio is about 31dB at 5GHz. In Fig. 3.7, the 10-dB impedance bandwidth is about 2.1GHz which is from 3GHz to 5.1GHz. Furthermore, the measurement results show that the F/B ratio is increased while the operating frequency is increased shown in Fig. 3.8.

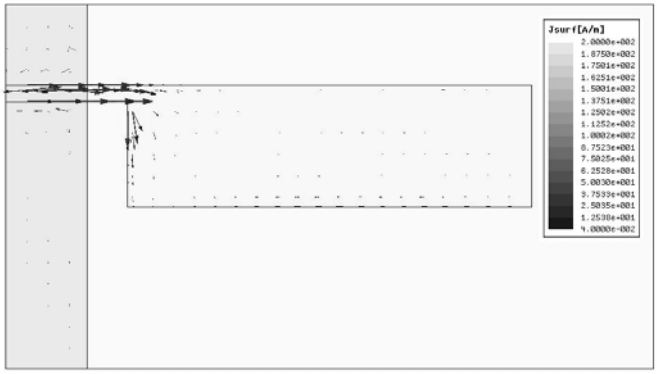

(a)

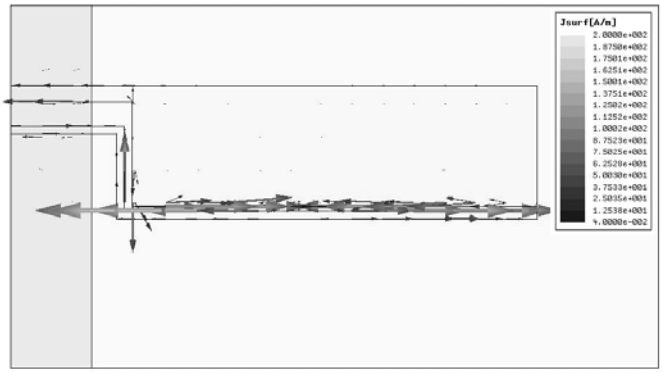

(b)

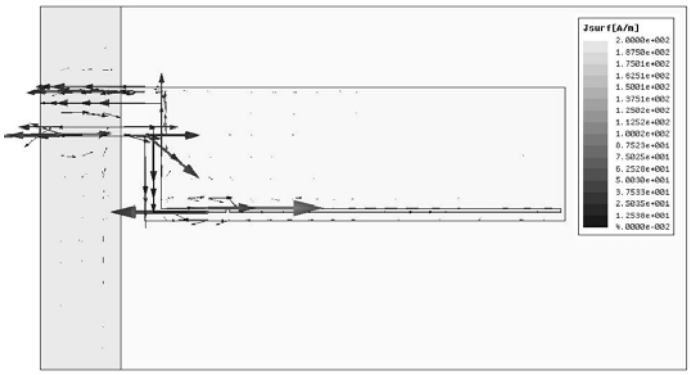

(c)

Fig. 3.5 The current distribution of the configuration

(a) Conventional open end leaky-wave antenna with reducing ground plane.

(b) Adding the stubs which are connected to the ground plane.

(c) Adding the connecting metal squares which connect the antenna body and the short-circuited stubs

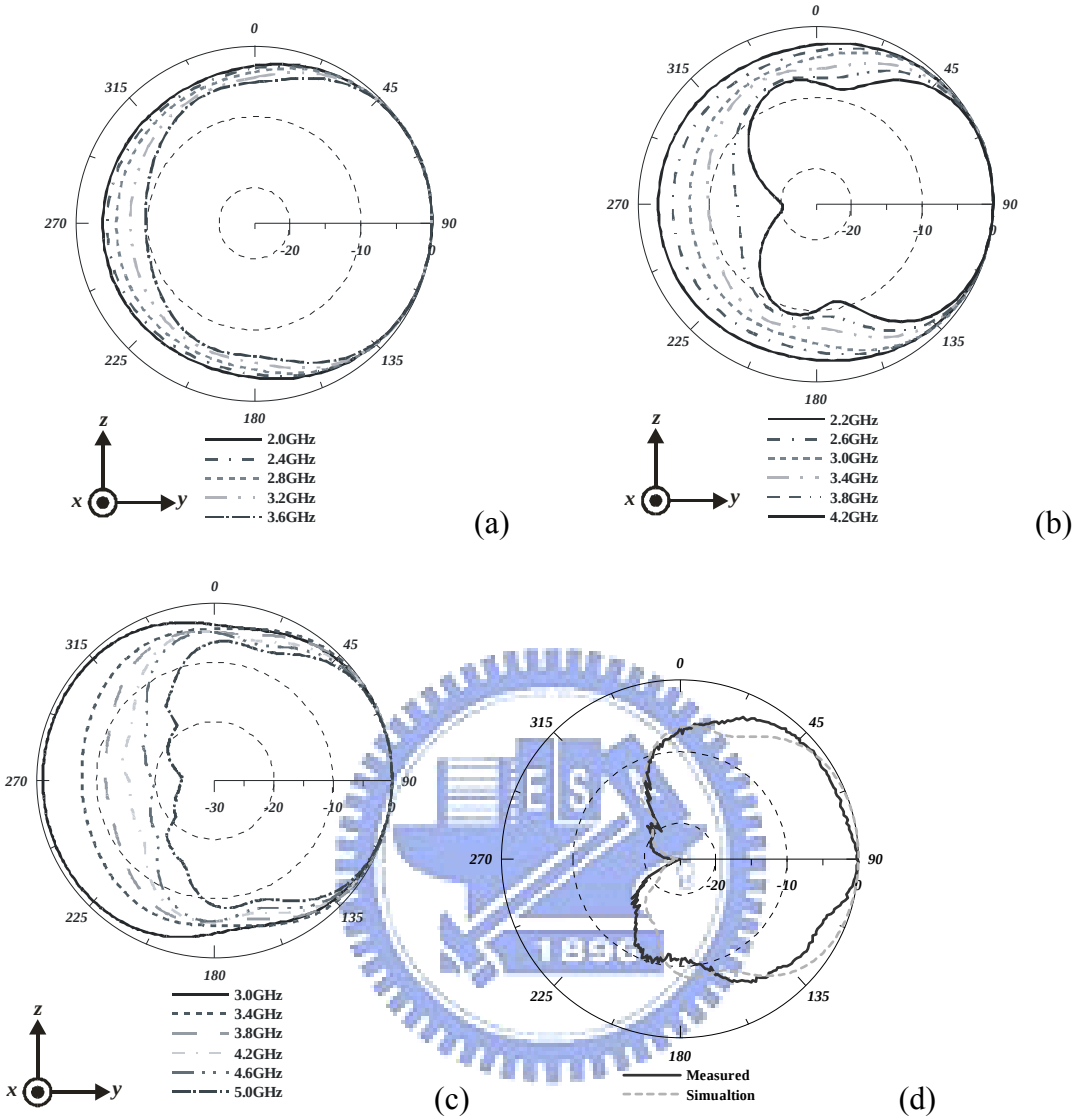

Fig. 3.6 The simulation normalized radiation pattern at its operating frequencies of the configuration

(a) Conventional open end leaky-wave antenna with reducing ground plane.

(b) Adding the stubs which are connected to the ground plane.

(c) Adding the connecting metal squares which connect the antenna body and the short-circuited stubs.

(d) Comparing the simulation and measured results of configuration (c) at 5GHz

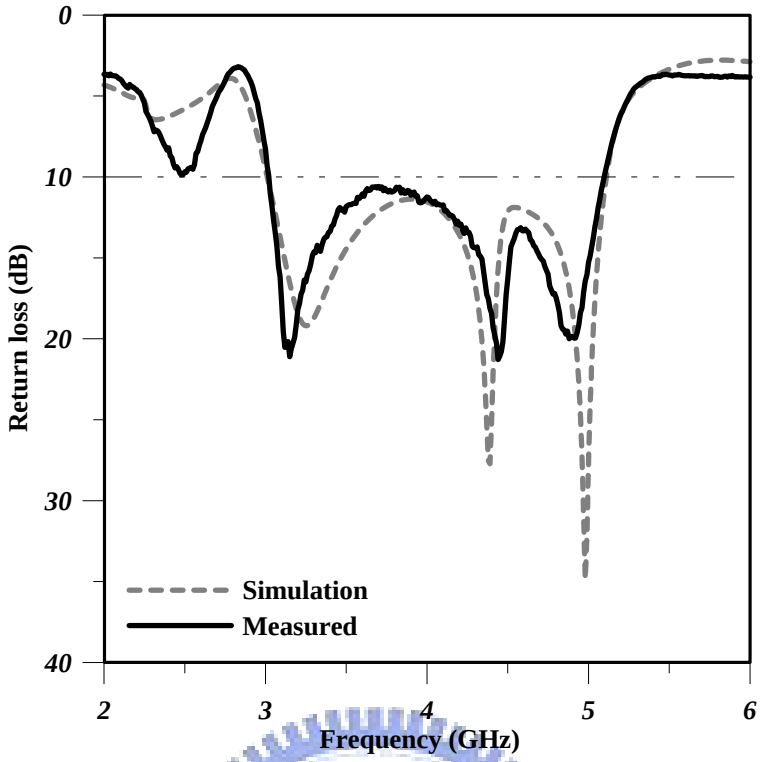

Fig. 3.7. The simulation and measured return loss of the configuration (c) of proposed antenna

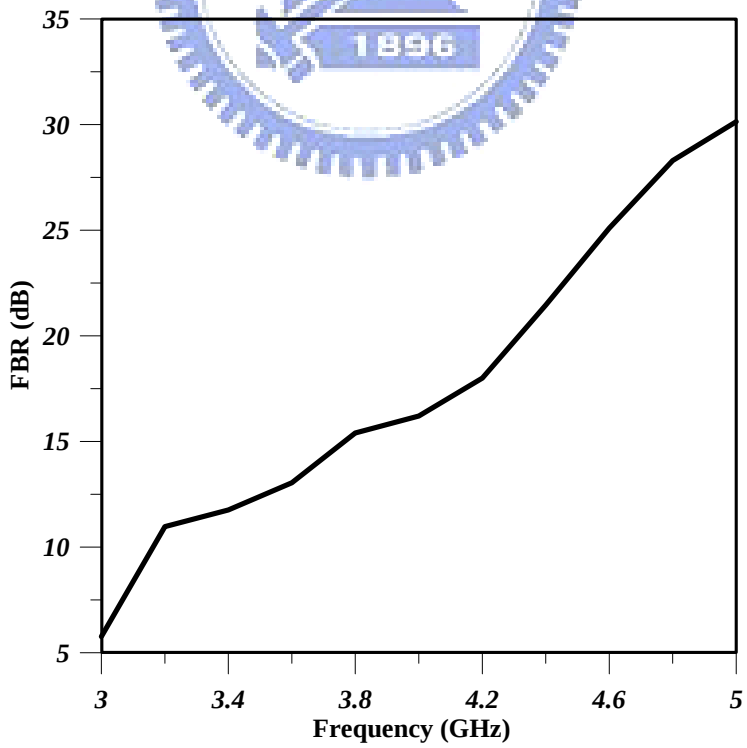

Fig. 3.8. The measurement F/B ratio of the configuration (c) of proposed antenna

3.4 Conclusion

A novel structure of the end-fire radiated antenna is present in this chapter. The impedance bandwidth of this antenna is about 51.8% at the center frequency of 4.05GHz for 10-dB return loss. The measurement peak antenna gain is about 5.4dBi. The F/B ratio of the proposed antenna configuration is increased while the operating frequency increased. The maximum F/B ratio is about 31dB at 5GHz. This proposed antenna structure is suitable for the many applications which require unidirectional radiation pattern such as traffic control, collision avoidance system, radiolocation, etc. and has great potential for applications in the future.

Chapter 4

High Front-to-Back Ratio Quasi-Yagi Antenna

In recent years, the quasi-Yagi antenna has become a major candidate for many applications because of its several advantages such as the good radiation performance. In this chapter, we will demonstrate the of the high front-to-back (F/B) ratio quasi-Yagi antenna whose the F/B ratio has been improved. We use the microstrip-fed structure of this quasi-Yagi antenna and adjust the position of the dipole arms, or the driver element, to improve the performance. And then, we will display the simulated and the measured results of this design.

4.1 Theory of Yagi-Uda Antenna [29]-[31]

The first research done on the Yagi-Uda antenna was performed by Shintaro Uda in 1926 and was published in Japanese in 1926 and 1927. The work of Uda was reviewed an article written in English by Uda's professor, H. Yagi, in 1928. [46]

The basic unit of a Yagi antenna has three elements: driver, reflector, and director. We can see the reflectors and the directors as the parasites of the array. When the parasitic element is put closely to the driver element, it is excited by the driver element with approximately equal amplitude and opposite in phase. According to the array theory, we can know that two closely spaced, equal amplitude, and opposite phase elements will have an end-fire pattern as shown in Fig. 4.1.

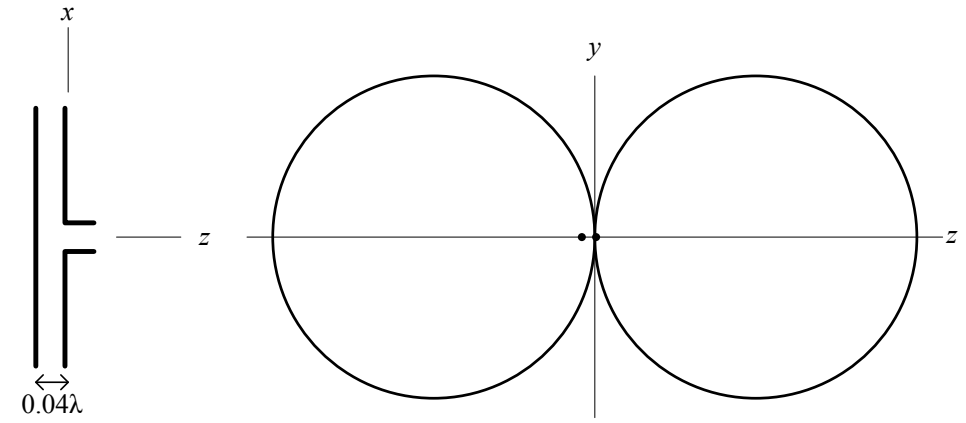

(a) (b)

Fig. 4.1 A two-element array of half-wave dipoles, one driver and the other parasite.

(a) Array configuration and (b) computed results of the *H*-plane pattern

However, the Yagi is revealed by the lengthening the parasite and then the dual endfire beam will change to a single endfire beam shown as in Fig. 4.2. Such a parasite element which is a few longer than the driver element is called a reflector because it appears to reflect radiation from the driver.

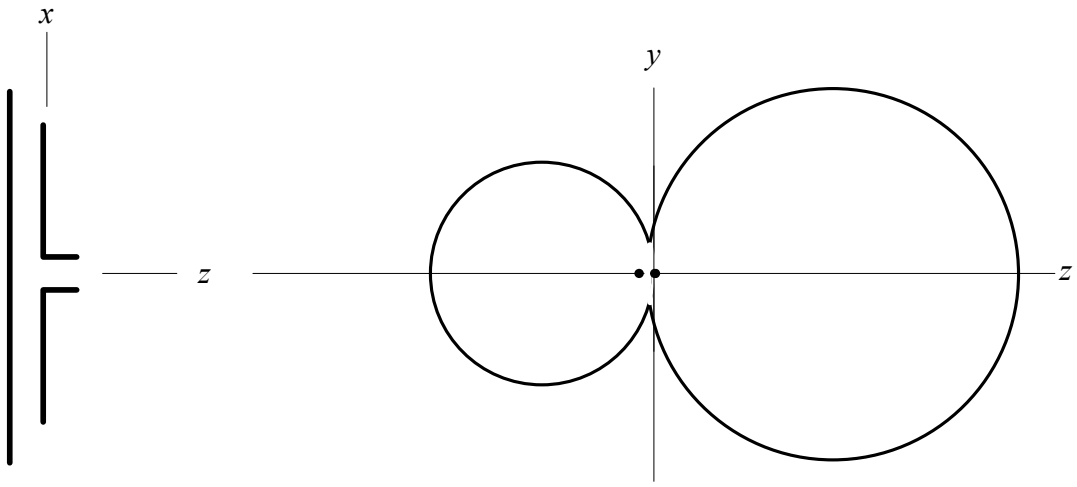

(a) (b)

Fig. 4.2 Two-element Yagi-Uda antenna consisting of a driver and a reflector

(a) Array configuration and (b) computed results of the *H*-plane pattern

If the parasite is shorter than the driver element, however, it placed on the other side of the driver, the radiation pattern is similar to that when using the reflector in the sense that the main beam will enhance in the same direction. So the parasite is called as a director because it appears to direct radiation in the direction from the driver to toward the director. Fig. 4.3(a) shows the parasitic array structure and the pattern of the structure which has a driver and a director is shown in Fig. 4.3(b).

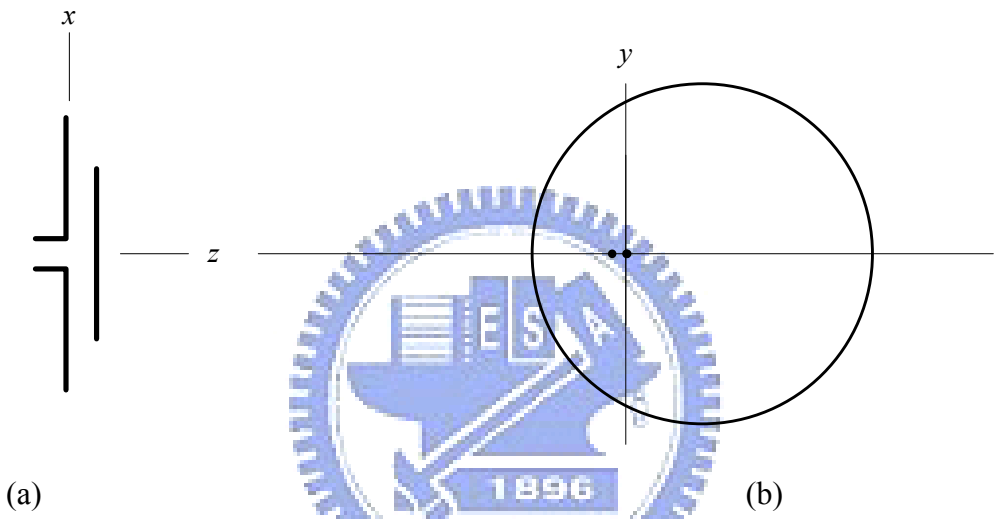

Fig. 4.3 Two-element Yagi-Uda antenna consisting of a driver and a director (a) Array configuration and (b) computed results of the *H*-plane pattern

According to the theory mentioned above, it suggests that we could enhance the antenna performance with a reflector and directors on the opposite sides of a diver. A general Yagi configuration which has a reflector, a driver, and several directors is shown in Fig. 4.4.

There are several design parameters of the Yagi antenna, such as the director-to-director, director-to driver, and driver-to-reflector spacing, and the number of the directors, which can improve the antenna gain, directivity, and front-to-back ratio.

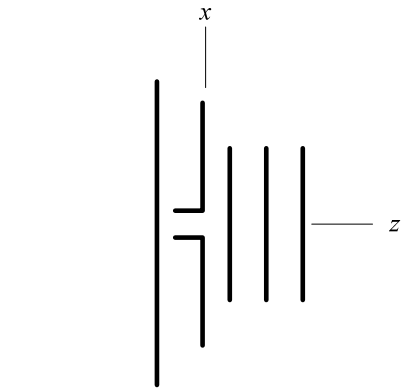

(a)

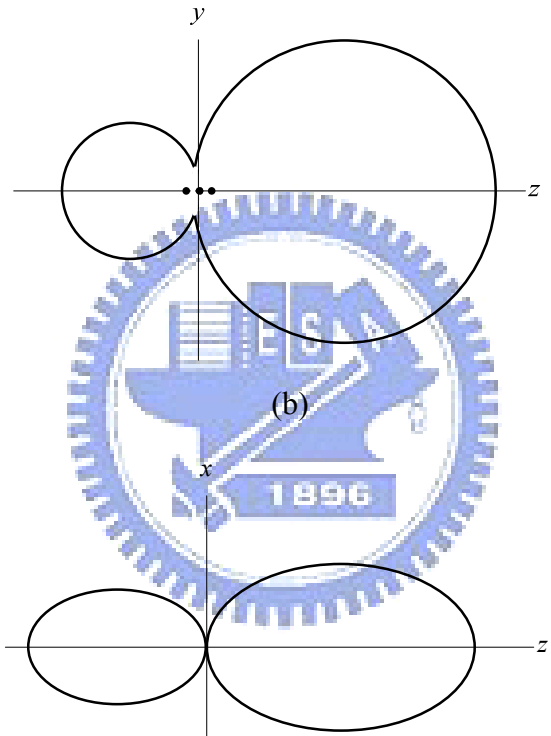

(b)

(c)

Fig. 4.4 Five-element Yagi-Uda antenna which has a driver, a reflector and three directors

(a) Array configuration,

(b) Computed results of the *H*-plane pattern and

(c) Computed results of the *E*-plane pattern

4.2 Design of the High F/BRatio Quasi-Yagi Antenna

The proposed antenna is printed on an FR4 substrate of the dielectric constant of 4.4, the conductor loss (tan δ) of 0.02, and the thickness of 1.6 mm. The structure of the antenna is shown in Fig. 4.5.

The antenna consists of three parts which are the reflector, or ground of the antenna, the driver, and the directors. For this design, it is called as quasi Yagi antenna whose radiation pattern is similar to the Yagi antenna, however, the structure of these two antennas are a little different.

Because the driver of the Yagi antenna is the half-wave dipole which needs differential excited, hence, we use the ground plane and the signal path to be the differential feed for this design [11]-[19]. That is to say, one of the dipole arms is extended from the ground plane of the microstrip structure and the other one is from the signal path as shown in Fig. 4.5.

It has three directors of this quasi Yagi antenna to improve the antenna gain and the F/B ratio [19]. Here, it is worth to be noticeable that the positions of the dipole arms are not at the symmetric location. The one extended from the ground plane is a few farther to the ground plane than the one extended from the signal path as shown in Fig. 4.6.

The antenna dimensional parameters values are as follows: W=40mm, L=20mm, W_s = 3 mm, L_1 = 8 mm, L_2 = 13 mm, W_{dri} =3 mm, L_{dri} = 14 mm, W_{dir} = 3 mm, L_{dir} = 14 mm and d = 1 mm. The total size is 60 $\times$ 40 mm^2.

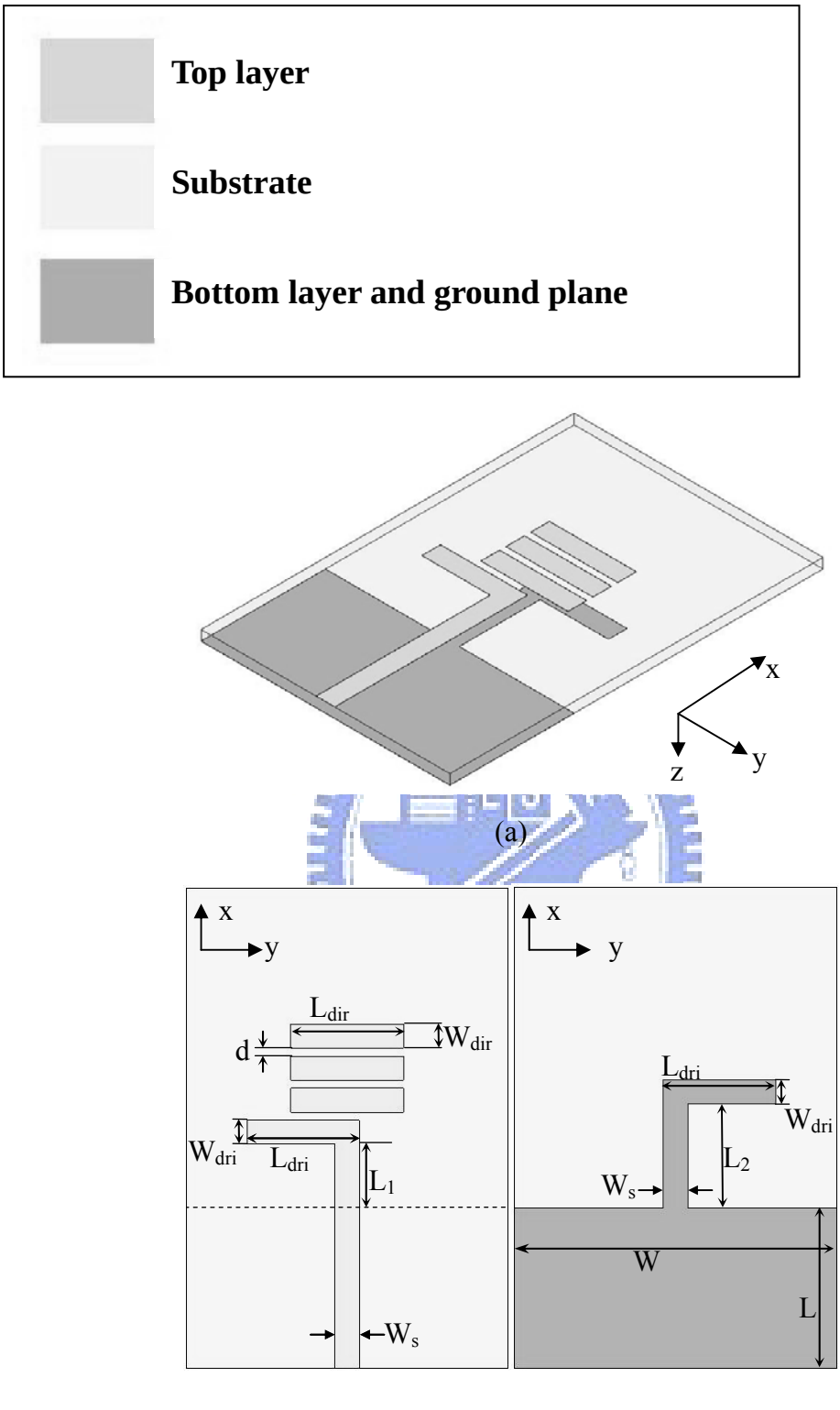

Fig. 4.5 Antenna geometry and parameters

(a)3D structure, (b) top layer and (c) bottom layer

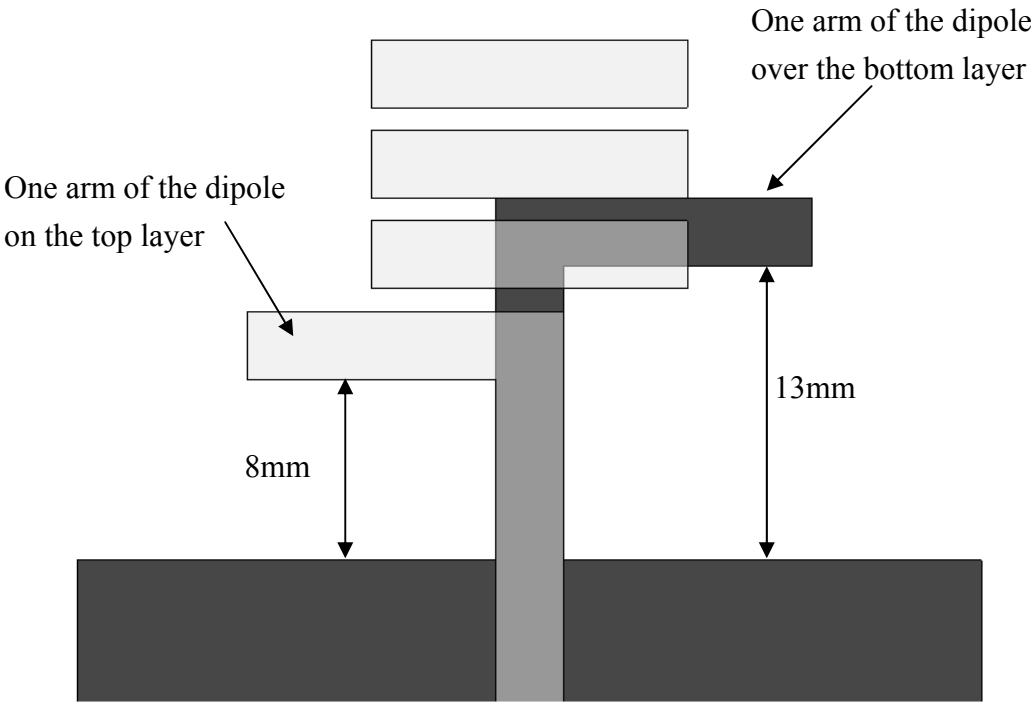

Fig. 4.6 The detail structure of the arms of the driver element

4.3 Simulation and Measurement Results for High F/B Ratio Quasi-Yagi Antenna

The return loss is computed using Ansoft HFSS [47] and measured using an 8510C vector network analyzer and is shown in Fig. 4.7. There are some small discrepancies between the simulated results and the measured results, which may occur due to the effect the SMA connector and fabrication imperfections. Both the simulation and the measurements show that the antenna operates over the range which extends from 3.9 GHz to 5.9 GHz with the impedance bandwidth of approximately 41% for this dipole arms quasi-Yagi antenna.

The simulated and the measured radiation patterns at the operating band center frequency, or 4.9 GHz, are shown in Fig. 4.8. The antenna has the 3-dB beamwidth that ranges from 142^{o} to 214^{o} in the XY-plane, or E-plane, and from 213^{o} to 332^{o} in the XZ-plane, or the H-plane.

Fig. 4.9 shows the measurement frequency dependence of the F/B ratio, which always exceeds the level of 20 dB. The measured antenna gain has an average value of 4 dBi.

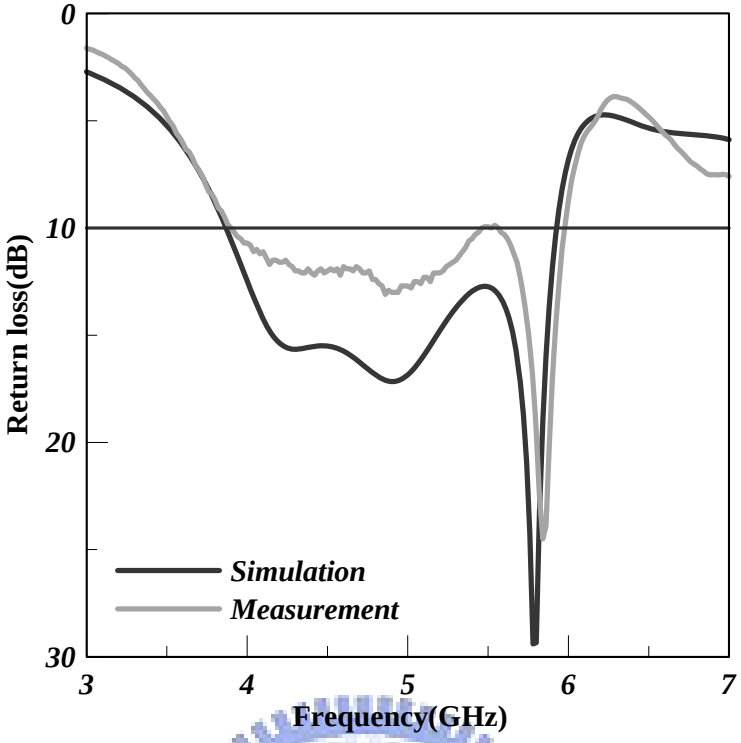

Fig. 4.7 Computed and measured return loss of the antenna

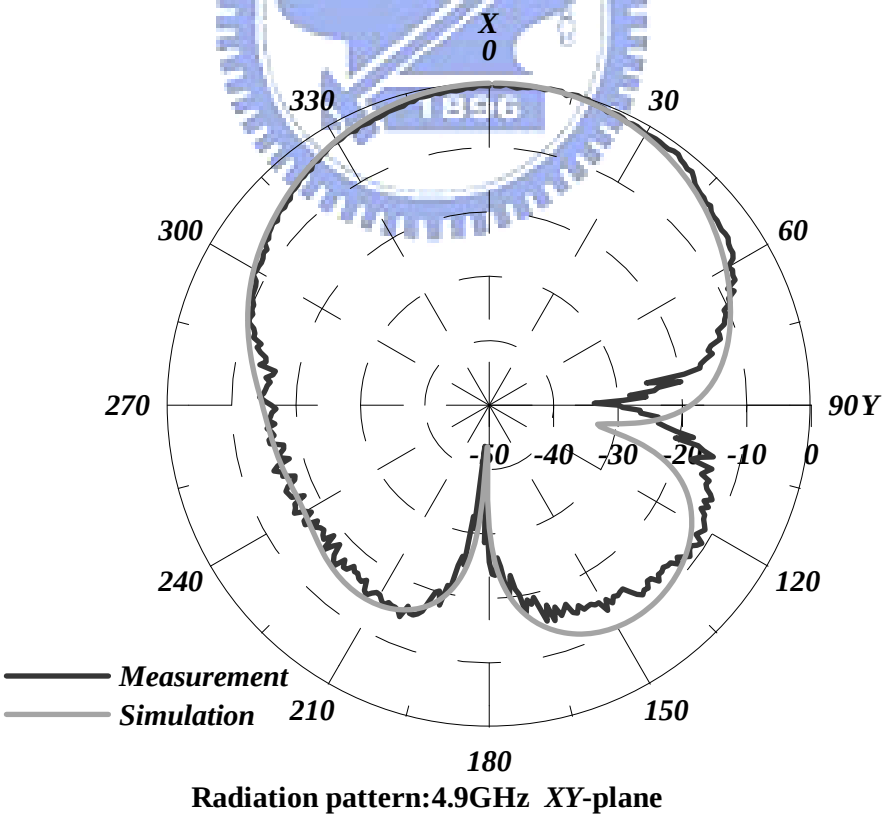

Fig. 4.8 Simulated and measured XY-plane radiation pattern at 4.9 GHz

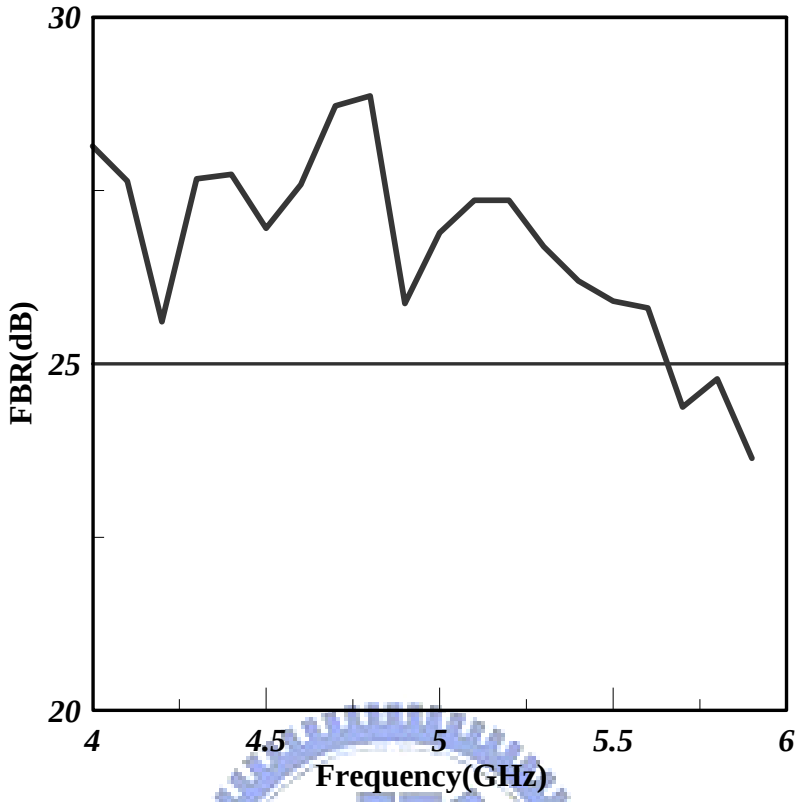

Fig. 4.9 Measured front-to-back ratio versus frequency

4.4 Design of the Enhance Type High F/B Ratio Quasi-Yagi Antenna

In order to increasing the F/B ratio, we proposed the enhance type antenna in which we added some directors and we adjusted the ground plane, or the reflector of this design. The antenna is also printed on an FR4 substrate of the dielectric constant of 4.4, the conductor loss (tan δ) of 0.02, and the thickness of 1.6 mm.

The difference between the prototype and the enhance type are the directors and the ground which is also the reflector of the antenna. The antenna gain will be higher if the mount of directors in more. Because of this reason, the enhance type one has eight directors totally, four of them are on the top layer and the other is on the backside of the substrate. For the ground plane, the right side is not symmetric to the left side. The structure of the antenna is shown in Fig. 4.10.

The antenna dimensional parameters values are as follows: W= 40 mm, L_1 =20 mm, L_2 = 22 mm, L_3 = 10 mm, L_4 = 8 mm, L_5 = 13 mm, L_6 = 31 mm, L_7 = 16 mm, d = 3 mm, d_1 = 1 mm, L_{d1} = 14 mm, L_{d2} = 12 mm, L_{d3} = 10 mm, L_{d4} = 8 mm. The total size is 60 $\times$ 40 mm^2.

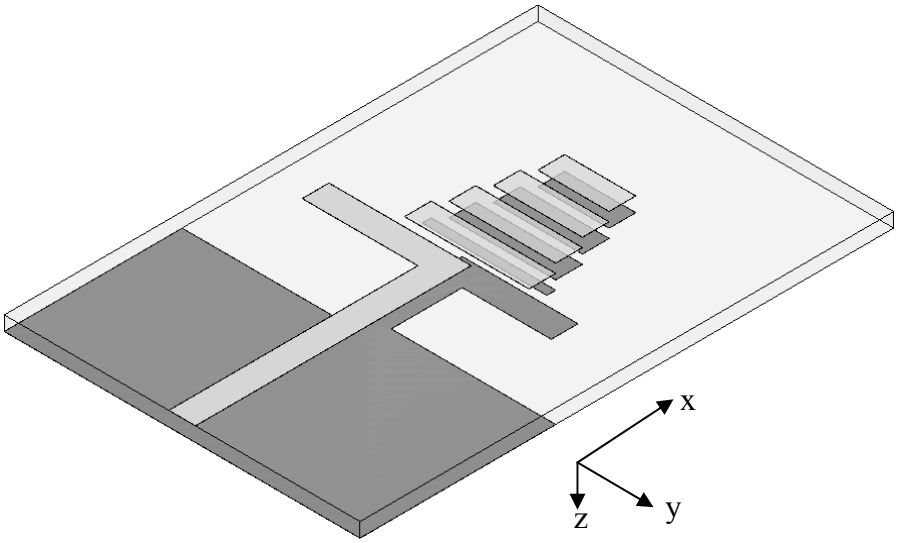

(a)

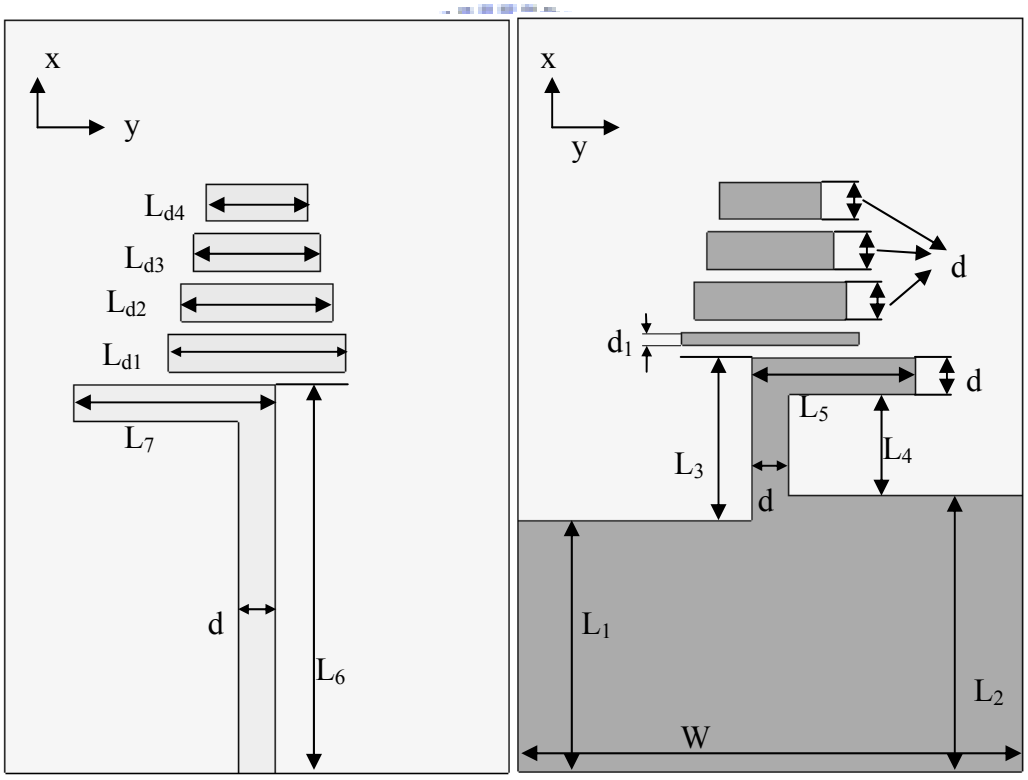

(b) (c)

Fig. 4.10 Antenna geometry and parameters

(a)3D structure, (b) top layer and (c) bottom layer

4.5 Simulation and Measurement Results for Enhance Type High F/B Ratio Quasi-Yagi Antenna

Fig. 4.11 shows that the measurement and the simulation return loss of the enhance type antenna. There are some discrepancies between the simulated results and the measured results, which may occur due to the effect the SMA connector and fabrication imperfections. Both the simulation and the measurements show that the antenna operates over the range which extends from 3.7 GHz to 6.5 GHz with the impedance bandwidth of approximately 55%.

The simulated and the measured radiation patterns at 5.5 GHz are shown in Fig. 4.12. The measured peak antenna gain is about 8.2 dBi. From the Fig. 4.12, we can see that the radiation pattern is the end-fire.

Fig. 4.13 shows the measurement frequency dependence of the F/B ratio, which exceeds 30dB even 40dB in the middle operating band.

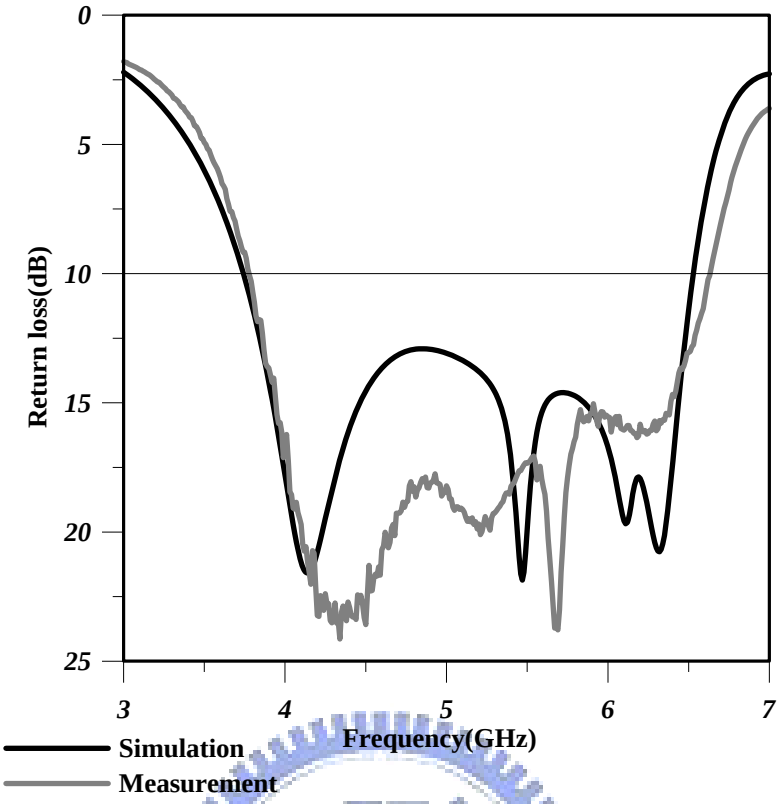

Fig. 4.11 Computed and measured return loss of the antenna

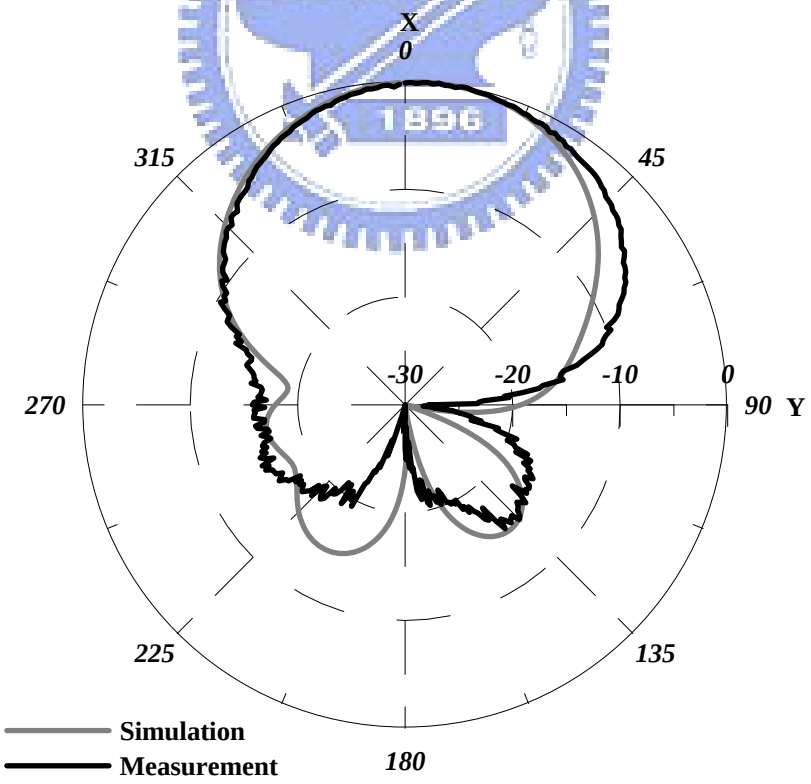

Fig. 4.12 Simulated and measured XY-plane radiation pattern at 5.5 GHz

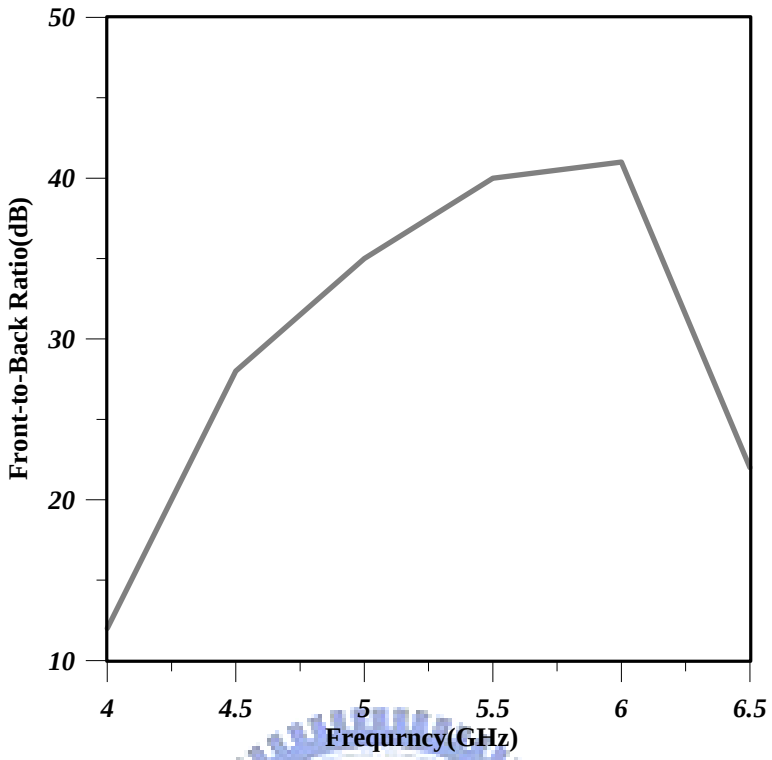

Fig. 4.13 Measured front-to-back ratio versus frequency

4.6 Conclusion

Here, a high F/B ratio quasi-Yagi antenna is designed and tested. This structure provides 41% impedance bandwidth (from 3.9 GHz to 5.9 GHz) which is better than the conventional symmetric position quasi-Yagi antenna. Meanwhile, it shows good radiation characteristics and can provide the average value of the antenna gain about 4 dBi. In the operating band, the F/B ratio always exceeds the level of 20 dB which achieves the purpose that is improving the unidirectional radiation pattern.

For the enhance type, the bandwidth is about 55% (from 3.7 GHz to 6.5 GHz). And its peak antenna gain can reach about 8.2 dBi. In the middle of operating band, the F/B ratio exceeds the level of 30 dB even 40dB which achieves the purpose that is improving the unidirectional radiation pattern better.

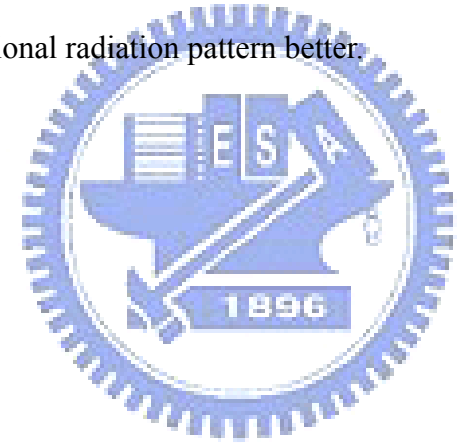

Chapter 5

Conclusion and Future Study

5.1 Conclusion and Summary

Here, we will summarize the conclusions of these two different topics. The first topic, on-chip antenna, has been integrated in the MMIC or the RFIC. It can provide the antenna radiation characteristics such as return loss, antenna gain, and radiation pattern. Moreover, because of the feed structure which is the CPW structure, it needs not the back metal process. So the implement has become more easily. In this design, it also shows the dual-band characteristics.

Then, the second topic, a novel structure antenna for end-fire antenna, we have demonstrated that the radiation pattern is the end-fire. Also, it has wide impedance bandwidth. And there is shown that the F/B ratio will increase while the operating frequency is increasing.

For the third topic, high F/B ratio quasi-Yagi antenna, we have shown that it can provide wide bandwidth and good radiation performance. And it always exceeds the level of 20 dB for the F/B ratio, which improves the unidirectional radiation characteristics. Here, in our design, the antenna can provide the gain about 4 dBi and the average F/B ratio is about 26 dB. And the enhance type, it also can provide wide bandwidth and good radiation performance which improves the unidirectional radiation characteristics better. The F/B ratio can exceed 30dB even 40dB in the middle of the operating band. The peak antenna gain can provide about 8.2 dBi.

5.2 Future Study

In the Future, there still have some topics we can research. For the on-chip antenna, how to increase the antenna gain, radiation efficiency, and how to design the antenna structure that can satisfy the IC design rule while the radiation pattern is we expected such topics are good researches. Another topic is that how to decrease the operating frequency band under the limit of the IC size condition.

Mentioning to the second topic, how to reduce the total size is one of the challenge need to be solved. And how to improve the bandwidth, antenna gain are also good researches.

For the quasi-Yagi antenna, how to improve the radiation performance is a good further research. Besides, enlarging the bandwidth, enhancing the antenna gain or increasing the directivity are also worthy to be studied.

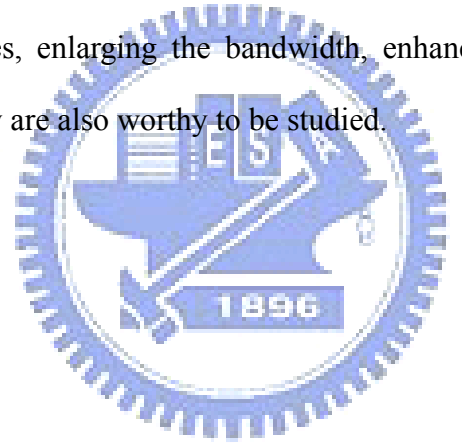

REFERENCE

[1] C.-C. Lin, S.-S. Hsu, C.-Y. Hsu, and H.-R. Chuang, "A 60-GHz Millimeter-wave CMOS RFIC-on-Chip Triangular Monopole Antenna for WPAN Applications," *IEEE Antennas Propag. International Symposium*, pp. 2522-2525, 9-15 Jun. 2007.

[2] S.-S. Hsu, K.-C. Wei, C.-Y. Hsu, and H.-R Chuang, "A 60-GHz Millimeter-Wave CPW-Fed Yagi Antenna Fabricated by Using 0.18-μm CMOS Technology," *IEEE Electron Device Lett.*, Vol. 29, Iss. 6, pp. 625-627, Jun. 2008.

[3] Federal Communications Commission, "Amendment of Parts 2, 15 and 97 of the Commission's Rules to Permit Use of Radio Frequencies Above 40 GHz for New Radio Applications", *FCC 95-499*, ET Docket No. 94-124, RM-8308, 15 Dec., 1995.

[4] A. Shamim, L. Roy, N. Fong, and N. G. Tarr, "24 GHz On-Chip Antennas and Balun on Bulk Si for Air Transmission," *IEEE Trans. Antennas Propag.*, vol. 56, no. 2, Feb. 2008.

[5] C. Cao, Y. Ding, X. Yang, J.-J. Lin, H.-T. Wu, A. K. Verma, J. Lin, F. Martin, K. O. Kenneth, "A 24-GHz Transmitter With On-Chip Dipole Antenna in 0.13-μm CMOS," *IEEE J. Solid-State Circuits*, vol. 43, Issue 6, pp.1394-1402, Jun. 2008.

[6] C. H. Doan, S. Emami, A. M. Niknejad, and R. W. Brodersen, "Design of CMOS for 60 GHz applications," *IEEE Solid-State Circuits Conf. Proc.*, pp. 440-449, 2004.

[7] Y. P. Zhang, M. Sun, and L. H. Guo, "On-chip antennas for 60-GHz radios in silicon technology," *IEEE Trans. Electron Devices.*, vol. 52, no. 7, pp. 1664-1668, Jul. 2005.

[8] M. Rahman, M. A. Stuchly, and M. Okoniewski, "Dual-band strip-sleeve monopole for handheld telephone," *Microwave Opt. Technol. Lett.*, vol. 21, no. 2, pp. 79-82, Apr. 1999.

[9] Y. P. Zhang, L. H. Guo, and M. Sun, "High transmission gain inverted-F antenna on low-resistivity Si for wireless interconnect," *IEEE Electron Device Lett.*, vol. 27, no. 5, pp. 374–376, May 2006.

[10] G.-W. Yao Z.-H. Xue, Z.-K. Liu, W.-M. Li, W. Nan, R. Wu, S.-M. Yang, "Design of high-directivity end-fire antenna array," *ICMMT International Conf. Proc.*, vol. 1, pp. 424-427, 21-24 Apr. 2008.

[11] S. Lim, “Design of a Multidirectional, High-Gain Compact Yagi Antenna,” *IEEE Antennas and Wireless Propag. Lett.*, vol. 8, pp. 418-320, 2009

[12] S. Lim and M. F. Iskander, “Design of a Dual-Band, Compact Yagi Antenna Over an EBG Ground Plane,” *IEEE Antennas and Wireless Propag. Lett.*, vol. 8, pp. 88-91, 2009

[13] T. T. Thai, G. R. DeJean and M. M. Tentzeris, “Design and Development of a Novel Compact Soft-Surface Structure for the Front-to-Back Ratio Improvement and Size Reduction of a Microstrip Yagi Array Antenna,” *IEEE Antennas and Wireless Propag. Lett.*, vol. 7, pp. 369-373, 2008

[14] S. E. Melais and T. M. Weller, “A Quasi Yagi Antenna Backed by a Metal Reflector,” *IEEE Trans. Antennas Propag.*, vol. 56, no. 12, pp. 3868–3872, Dec. 2008

[15] G. R. DeJean, “A new steerable Yagi antenna array for indoor applications,” *Proc. IEEE AP-S Int. Symp.,* pp. 1-4, 5-11 Jul. 2008

[16] X.-S. Yang, B.-Z. Wang, W. Wu and S. Xiao, “Yagi Patch Antenna With Dual-Band and Pattern Reconfigurable Characteristics,” *IEEE Antennas and Wireless Propag. Lett.*, vol. 6, pp. 168-171, 2007

[17] G. R. DeJean and M. M. Tentzeris, “A New High-Gain Microstrip Yagi Array Antenna With a High Front-to-Back (F/B) Ratio for WLAN and Millimeter-Wave Applications,” *IEEE Trans. Antennas Propag.*, vol. 55, no. 2, pp. 298–304, Feb. 2007

[18] S.-Y. Chen and P. Hsu, “Broadband Microstrip-Fed Modified Quasi-Yagi Antenna,” *IEEE/ACES International Conf.*, pp. 208-211, 3-7 Apr. 2005

[19] G. Zheng, A.A. Kishk, A.W. Glisson and A.B. Yakovlev, “Simplified feed for modified printed Yagi antenna,” *IEEE Electronics Lett.*, vol. 40, Iss. 8, pp. 464–466, Apr. 2004.

[20] C. P. Wen, “Coplanar waveguide: a surface strip transmission line suitable for nonreciprocal gyromagnetic device applications,” *IEEE Trans. Microw. Theory Tech.*, vol. 17, no. 12, pp. 1087-1090, Dec. 1969

[21] J. L. B. Walker, “A Survey of European Activity on Coplanar Waveguide,” *IEEE MTT-S Int. Microwave Symp. Dig.*, Vol. 2, pp. 693-696, Atlanta, Georgia, 14-18 Jun. 1993

[22] A. K. Sharma and T. Itoh (Editors), Special Issue on Modeling and Design of Coplanar Monolithic Microwave and Millimeter-Wave Integrated Circuits, *IEEE Trans. Microwave T heory Tech.*, vol. 41, no. 9, Sep. 1993.

[23] T. Sporkmann, “The Evolution of Coplanar MMICs over the past 30 Years,” *Microwave J.*, vol. 41, no. 7, pp. 96-111, Jul. 1998.

[24] T. Sporkmann, “The Current State of the Art in Coplanar MMICs,” *Microwave J.*, vol. 41, no. 8, pp. 60-74, Aug. 1998.

[25] J. Browne, “Broadband Amps Sport Coplanar Waveguide,” *Microwaves RF*, vol. 26, no. 2, pp. 131-134, Feb. 1987.

[26] J. Browne, “Coplanar MIC Amplifier Bridges 0.5 To 18.0 GHz,” *Microwaves RF*, vol. 26, no. 6, pp. 194-195, Jun. 1987.

[27] R. E. Stegens and D. N. Alliss, “Coplanar Microwave Integrated Circuit for Integrated Subsystems,” *Microwave Sys. News Comm. Tech.*, vol. 17, no. 11, pp. 84-96, Oct. 1987.

[28] R. N. Simons, *Coplanar Waveguide Circuits, Components, and Systems*, 1st ed. New York: John Wiley & Sons, 2001.

[29] W. L. Stutzman and G. A. Thiele, *Antenna Theory and Design*, 2nd ed. New York: John Wiley & Sons, 1998

[30] C. A. Balanis, *Antenna Theory Analysis and Design*, 3rd ed. New York: John Wiley & Sons, 2005.

[31] J. D. Kraus, *Antennas for all applications*, 3rd ed. New York: McGraw-Hill, 2002

[32] H.-R. Chuang and L.-C. Kuo, “ 3-D FDTD design analysis of a 2.4 GHz polarization-diversity printed dipole-antenna with integrated balun and polarization-switching circuit for WLAN and wireless communication applications, ” *IEEE Trans. Microw. Theory Tech.*, vol. 51, no. 2, pp. 374–381, Feb. 2003.

[33] L.-C. Kuo and H.-R. Chuang, “A study of printed dipole antennas for wireless communication applications,” *J. Electromagn. Waves Appl.*, vol. 21, no. 5, pp. 637–652, Jan. 2007.

[34] D. Bhattacharya, “Characteristic Impedance of Coplanar Waveguide,” *Electronics Lett.*, vol. 21, Iss. 13, pp. 557, Jun. 1985.

[35] N. Gokalp and O. A. Civi, “Beam steerable traveling wave meander line antenna using varactor diode for X-band applications,” *Proc. IEEE AP-S Int. Symp.,* pp. 1-4, 5-11 Jul. 2008

[36] I. Hertl and M. Strycek, “Tapered slot antenna with reduced backward radiation,” *Micow., Radar and Wireless Communications Conf.* pp. 1-4, 19-21 May, 2008

[37] S. K. Podilchak, A. P. Freundrofer and Y. M. M. Antar, “Planar antenna for directive beam steering at end-fire using an array of surface-wave launchers,” *IEE Electron Lett.*, vol. 45 no. 9, pp. 444-445, Apr. 2009

[38] G.-W. Yao, Z.-H. Xue, Z.-K. Liu, W.-M. Li, W. Nan, R. Wu, S.-M. Yang, "Design of high-directivity end-fire antenna array," *ICMMT International Conf. Proc.*, vol. 1, pp. 424-427, 21-24 Apr. 2008.

[39] A. A. Oliner and K. S. Lee, "Microstrip leaky wave strip antennas," *IEEE AP-S Int. Symp. Dig.*, Philadelphia, PA, June 1986, pp. 443–446

[40] Y. Li, Q. Xue, E. K.-N. Yung and Y. L. Long, "Radiation patterns of microstrip leaky-wave antenna with parasitic elements," *Microw. Opt. Technol. Lett.,* vol. 50, no. 6, pp. 1565-1567, Jun. 2008

[41] Y. Li, Q. Xue, E. K.-N. Yung and Y. Long, "A Fixed-Frequency Beam-Scanning Microstrip Leaky Wave Antenna Array," *IEEE Antennas and Wireless Propag. Lett.*, vol. 6, pp. 616-618, 2007

[42] Y. Li, Q. Xue, E. K.-N. Yung and Y. Long, "Fixed-Frequency Dual-Beam Scanning Microstrip Leaky Wave Antenna," *IEEE Antennas and Wireless Propag. Lett.*, vol. 6, pp. 444-446, 2007

[43] http://www.jedsoft.org/fun/antennas/yagi.html

[44] http://hf-ssb-transceiver.at-communication.com/en/hf_ssb_antennas_stationary.html

[45] http://www.analyzemath.com/antenna_tutorials/antenna_arrays.html

[46] H. Yagi. "Beam Transmission of Ultra-short Waves," *Proc. IRE*, vol. 16, p. 715, 1928

[47] HFSS: High Frequency Structure Simulator Based on the Finite Element Method. Ansoft